Human milk extracellular vesicles survive neonatal digestion in vivo to be absorbed by neonatal enteroids

Yang Zhang[1], Madeline Kuhn[1], Claire Yung[1], Randall J. Armstrong[2,3], Amy Olyaei[4], Molly Aloia[4], Brian Scottoline[1,4], and Sarah F. Andres[1]*.

[1]Department of Pediatrics, Pediatric GI Division, School of Medicine, [2]Knight Cancer Institute, [3]Cancer Early Detection Advanced Research (CEDAR), [4]Division of Neonatology, Department of Pediatrics, Oregon Health and Science University, Portland, OR, USA 97229

*corresponding author, andress@ohsu.edu

Keywords (max of 6)

Human milk, digestion, neonatal enteroids, extracellular vesicles, necrotizing enterocolitis, absorption

ABSTRACT

Human milk contains extracellular vesicles (HMEVs). Pre-clinical models suggest that HMEVs may enhance intestinal function and limit inflammation; however, it is unknown if HMEVs or their cargo survive neonatal human digestion. This limits the ability to leverage HMEV cargo as additives to infant nutrition or as therapeutics. This study aimed to develop an EV isolation pipeline from small volumes of human milk and neonatal intestinal contents after milk feeding (digesta) to address the hypothesis that HMEVs survive in vivo neonatal digestion to be taken up intestinal epithelial cells (IECs). Digesta was collected from nasoduodenal sampling tubes. EVs were isolated from raw and pasteurized human milk and digesta by density-gradient ultracentrifugation following two-step skimming, acid precipitation of caseins, and multi-step filtration. EVs were validated by electron microscopy, nanoparticle tracking analysis, and western blotting. EV uptake and effects were tested in human neonatal enteroids. HMEVs and digesta EVs (dHMEVs) show typical EV morphology and are enriched in CD81 and CD9, but depleted of β-casein and lactalbumin. HMEVs and dHMEVs contain mammary gland-derived protein BTN1A1. Neonatal human enteroids rapidly take up dHMEVs in part via clathrin-mediated endocytosis. Our data suggest that HMEVs survive to the duodenum and can be absorbed by IECs.

35 **1. INTRODUCTION**

36 Human milk (HM) contains numerous bioactive factors with nutritive and
37 nonnutritive benefits to promote the health and long-term well-being of the developing
38 infant (1). For example, feeding human milk enhances intestinal function and reduces
39 the risk of necrotizing enterocolitis (2-10), promotes healthy brain development (11), and
40 reduces the risk of chronic disorders, such as asthma or inflammatory bowel disease
41 (12).

42 Human milk is replete with extracellular vesicles (EVs), which are nanoparticle-
43 sized structures secreted by most cells within the human body (13). EVs, including
44 human milk EVs (HMEVs), carry biological information between donor and recipient
45 cells, to confer changes in cellular function or biological activity (14-22). HMEVs have
46 putative beneficial effects, as shown by a combination of in vitro and animal studies
47 demonstrating that HMEVs promote intestinal epithelial cell proliferation (16, 19, 20),
48 reduce experimental necrotizing enterocolitis (NEC), limit inflammatory (15-17, 21, 22) or
49 non-inflammatory damage (15, 19, 23), promote expression of intestinal barrier proteins
50 (21), or enhance epithelial barrier function (15, 18). Collectively, the data suggest that
51 HMEVs confer functional benefits on intestinal epithelial cells (IECs) and hold immense
52 therapeutic promise for humans. To do so, however, HMEVs must survive infant
53 digestion to reach the intestinal epithelium.

54 Several in vitro studies indicate that HMEVs are minimally impacted by a pH of 4-
55 4.5 mirroring that of a term or preterm infant stomach, as well as incubation with several
56 gastrointestinal proteases (24-26). More recent work shows that bovine milk EVs are
57 intact after exposure to a pH as low as 1.3 (15). Furthermore, existing animal studies
58 indicate that bovine or murine milk-derived EVs survive murine digestion to reach the
59 placenta and embryo (27) or intestine and brain (28, 29). Studies also demonstrate that
60 HMEVs confer beneficial effects within the murine intestine (15, 17, 21), suggesting that

61 they too may survive murine digestion. Yet it remains unknown if HMEVs survive
62 neonatal human digestion to functionally impact the neonatal human intestinal
63 epithelium. Answering this question is a critical next step for understanding the ability to
64 orally deliver HMEVs as therapeutics or drug carriers.

65 The neonatal intestinal epithelium is thought to take up macromolecules through
66 bulk endocytosis (30, 31), a mechanism unique to the neonate where endocytic cargo is
67 broken down by the lysosome. Existing data similarly suggest that endocytosis is the
68 primary mechanism of EV uptake, although precise mechanisms may vary depending on
69 the cell of EV origin and the acceptor cell type (32, 33). Studies examining bovine milk
70 EV uptake in mice or human cell lines (Caco2) indicate that the FcRn receptor plays a
71 role in the uptake of some milk EVs (34, 35).

72 Studies examining HMEV uptake are limited and use transformed IEC lines, such
73 as Caco2 (24) or HIEC (25) cells. Although these cell lines are commonly used to model
74 the small intestinal epithelium (36, 37), Caco2 cells are derived from human colorectal
75 cancer (38, 39), while HIEC cells are derived from 17-19 week fetal ileum (40). To date,
76 the uptake of HMEVs by primary, human neonatal IECs remains unexplored.

77 In this study, we hypothesized that a proportion of HMEVs in human milk survive
78 in vivo infant digestion to reach the small intestine and be taken up by IECs. To test this
79 hypothesis, we utilized a rare and valuable set of fed human milk and intestinal contents
80 (digesta) samples isolated from infants in the neonatal intensive care unit (NICU). We
81 optimized a relatively high-purity EV isolation pipeline allowing for the isolation of
82 HMEVs from 1 mL of raw human milk (RHM), pasteurized donor human milk (PDHM), or
83 digesta. We also developed and characterized a primary human neonatal enteroid
84 culture system to examine digested HMEV (dHMEV) uptake ex vivo. Enteroids are 3D
85 organoid cultures grown from intestinal stem cells (41, 42). In contrast to immortalized
86 cell lines used in previous studies (24, 25), primary neonatal enteroids are arguably a

87 more physiologically relevant model for studying normal IEC function (43) as they are
88 derived from normal infant intestinal stem cells and develop multiple differentiated IEC
89 types.

90 Our data demonstrate for the first time that a proportion of HMEVs can survive in
91 vivo neonatal digestion. These dHMEVs are readily and robustly endocytosed by
92 neonatal enteroids containing differentiated IECs, primarily via dynamin-dependent
93 processes. This study addresses a critical gap in understanding the potential role(s) of
94 HMEVs in the infant intestine and in the pipeline for HMEV therapeutic development.

95 2. MATERIALS AND METHODS

96 All human studies were approved by the Oregon Health & Science University (OHSU)
97 Institutional Review Board (IRB) IRB #17968 and #21952. All milk, digesta, and tissue
98 samples were collected after obtaining parental informed consent.

99 2.1 Sample collection

100 Human milk samples, collection, and storage are listed in **Table 1**. All samples were
101 aliquoted and frozen before processing and every effort was taken to minimize freeze
102 thaws. Raw human milk (RHM) or pasteurized donor human milk (PDHM) collection was
103 performed under OHSU IRB #17968. PDHM was obtained from the Northwest Mother's
104 Milk Bank (Beaverton, OR, USA) or Prolacta (City of Industry, CA, USA).

105 In vivo, digested milk samples (digesta) were collected from infants in the
106 Doernbecher Children's Hospital NICU at OHSU under IRB #17968. Infant inclusion
107 criteria were: infants already admitted to the NICU, greater than 26 weeks corrected
108 gestational age, an indwelling nasogastric or orogastric feeding tube, and tolerating full
109 enteral feeding volumes. Infants were excluded from the study if they had anatomic or
110 functional gastrointestinal disorders that would affect digestion, were medically unstable,

111 or were non-viable. Digested milk samples were collected from three infants (**Table 1**).
112 Before feeding, a nasal tube was placed into the duodenum or proximal jejunum. Feeds
113 were delivered via a gastric tube over 30 min or less. Samples were collected from the
114 nasojejunal/duodenal tube via gravity flow as the digesta passed the post-pyloric collection
115 tube port into sterile vials, placed on ice, aliquoted, and stored at –80 °C.
116

117 **2.2 Isolation of extracellular vesicles from human milk and neonatal digesta**

118 Samples were quickly thawed in a 37 ºC water bath and used immediately (44, 45). A
119 step-by-step illustration is depicted in **Figure 1**. One milliliter of RHM, PDHM, or digesta
120 was used for each isolation. Samples were centrifuged at 6,000 x g for 10 min at 4 ºC to
121 remove cream and large cellular debris (46). The supernatant was carefully collected
122 and centrifuged again at 2,000 x g for 20 min at 4 ºC to further remove any fat globules
123 and/or smaller cellular debris. This supernatant was then passed through Whatman™
124 Grade 1 filter paper (diameter 42.5 mm) using a glass funnel before isoelectric casein
125 precipitation.

126 Acetic acid (1 and 10 N) was used to adjust the pH of the supernatant (initial pH
127 6.8 - 7.4) to 4.6 using a portable pH meter (Southern Labware, Fisher Scientific,
128 Hampton, NH, USA). Acetic acid was added to samples ≤1 µL at a time, and samples
129 were briefly mixed after each acid addition. Once the pH was adjusted to 4.6, samples
130 were incubated at room temperature for 10 min before final centrifugation at 5,000 x g
131 for 30 min at 4 ºC. The supernatant was carefully collected and was passed through
132 Whatman™ Grade 1 filter paper (diameter 42.5 mm) using a glass funnel, a 0.45 µm
133 syringe filter, and a 0.22 µm syringe filter for the further removal of casein residue
134 yielding clarified HM or digesta.

135 Density gradient ultracentrifugation using a SW Type 55 Ti swinging bucket rotor
136 in LM-70 ultracentrifuge (Beckman Coulter, Brea, CA, USA) was achieved using

137 OptiPrep™ iodixanol solution (60% iodixanol, w/v) following the bottom-up technique
138 (47). A 45% (w/v) bottom layer was made by diluting OptiPrep™ solution with clarified
139 HM or digesta sample (2.25 mL OptiPrep™ + 0.75 mL sample = 3 mL) into a 5 mL open-
140 top thin wall ultra-clear tube (Beckman Coulter). A discontinuous gradient was made with
141 40% (w/v), 30% (w/v), 20% (w/v) and 10% (w/v) solutions of iodixanol (diluted with
142 sterile, 0.1 µm-filtered phosphate-buffered saline (PBS)) carefully layered on top of the
143 prior density, drop by drop. The ultracentrifugation was carried out at 169,522 × g
144 (37,400 rpm) for 24 hours at 4 ºC with zero acceleration and deceleration. After
145 ultracentrifugation, 500 µL fractions were carefully collected into protein LoBind tubes
146 (Fisher) from top to bottom using a P1000 pipette without disrupting the layers. The
147 fractions were used the same day for analysis or functional studies. We submitted all
148 relevant data of our experiments to the EV-TRACK knowledgebase (EV-TRACK ID:
149 EV230590) (48).
150
151 **2.3 Cell Lines**
152 SW480 and MCF7 cells (western blot positive controls) were cultured in DMEM high
153 glucose medium (Gibco, Thermo Fisher, Waltham, MA, USA) supplemented with 10%
154 fetal bovine serum (FBS, Cytiva HyClone™, Marlborough, MA, USA) and 1%
155 penicillin/streptomycin (Gibco), and grown at 37 ºC in a humidified incubator with 5%
156 CO_2. Cells were lysed in radioimmunoprecipitation assay-sodium dodecyl sulfate (RIPA-
157 SDS) and protein concentration was quantified using a bicinchoninic acid (BCA) reagent
158 kit (Thermo Fisher, Waltham, MA, USA) following manufacturer instructions ahead of
159 western blotting.
160
161 **2.4 Validation of extracellular vesicle isolation**

162 **2.4.1 Western blotting**

163 For validation, EV preparations and cellular controls were lysed in 6X Laemmli buffer
164 (375 mM Tris-HCl pH 6.8, 9% SDS w/v, 50% Glycerol v/v, 0.03% Bromophenol blue w/v,
165 9% DTT w/v), incubated at 37 ºC for 30 min, and loaded onto 4 to 12% Bis-Tris mini
166 protein gels (NuPAGE™, Invitrogen, Waltham, MA, USA, 1.5 mm). PageRuler Plus™
167 Prestained Protein Ladder (Thermo Fisher, 10 – 250 kDa) was resolved as a molecular
168 weight reference. Human cell lines, MCF7 (breast cancer) (ATCC) and SW480
169 (colorectal cancer) (ATCC) were also resolved as cellular controls. The ATCC
170 authenticates all human cell lines through short tandem repeat analysis. All cell lines
171 were confirmed to be mycoplasma negative every 3 weeks (MycoAlert™ Mycoplasma
172 Detection Kit, Lonza, Bend, OR, USA). Fifteen micrograms of total whole cell lysates
173 (WCL) and 20 µL of EV lysate isolated from 1 mL starting volume were resolved by gel
174 electrophoresis. The samples were stacked for 30 min at 60V and resolved for 60 min at
175 150V in 1X NuPAGE™ MOPS SDS running buffer (Invitrogen) and transferred onto
176 0.45µm PVDF membrane (Immobilon, Millipore/Merck) via a wet transfer system with 1X
177 NuPAGE™ transfer buffer (Invitrogen) at 100 V for 60 min. Membranes were blocked
178 with LI-COR PBS blocking buffer (LI-COR, Lincoln, NE) at room temperature for 60 min.

179 MISEV 2018 guidelines (13) were used to characterize the presence of EV-
180 specific proteins via the following primary antibodies: 1) anti-transmembrane protein
181 markers: anti-CD9 (rabbit, Abcam, Cambridge, UK, ab236630 1:1000); anti-CD63
182 (rabbit, System Biosciences, Palo Alto, CA, USA, EXOAB-CD63A-1, 1:1000); anti-CD81
183 (mouse, Santa Cruz Biotechnology, sc-166029, 1:1000), and 2) cytosolic protein
184 markers: anti-TSG101 (mouse, BD Biosciences, Franklin Lakes, NJ, USA, 612697,
185 1:1000) and anti-FLOT1 (rabbit, Cell Signaling Technology, 3253S, 1:10,000-1:15,000).
186 Lactating mammary gland protein butyrophilin (BTN1A1) anti-BTN1A1 (mouse, OriGene
187 Technologies, Rockville, MD, USA, TA501529S 1:3000). Anti-ITGB1, (rabbit, Cell

188 Signaling Technology, Danvers, MA, USA, 34971T, 1:1000) was used to identify
189 microvesicle contamination (49). Anti-GM130 (rabbit, Novus Biologicals, Centennial, CO,
190 USA, NBP2-53420, 1:1000) was used to identify cis-Golgi matrix protein as a marker of
191 cellular contamination (13). Anti-LALBA (rabbit, Abcam, ab178431, 1:1000) and anti-
192 CSN2 (rabbit, Abcam, ab205301, 1:5000) assessed non-HMEV components from
193 lactalbumin and casein, respectively. All primary antibodies were diluted in 0.5X LI-COR
194 PBS blocking buffer (LI-COR Biosciences, Lincoln, NE, USA) diluted with 1X PBS
195 containing 0.2% tween-20.
196 The membranes were incubated with goat anti-rabbit labeled with IRDye 700
197 (1:20 000, v/v, LI-COR) and/or goat anti-mouse antibody labeled with IRDye 800
198 (1:20,000, v/v, LI-COR) for 60 min before visualization on LICOR Odyssey. All
199 secondary antibodies were diluted in 0.5X LI-COR PBS blocking buffer diluted with 1X
200 PBS containing 0.2% tween-20 and 0.01% sodium dodecyl sulfate (SDS).
201
202 **2.4.2 Nanoparticle Tracking Analysis**
203 All samples were diluted in 10% particle-free PBS (Genesee Scientific, Morrisville, NC,
204 USA) to a final volume of 1 mL. Samples were diluted to achieve 50 – 250
205 particles/frame) before injection (50). Samples were analyzed using a ZetaView® Twin
206 (Particle Metrix, Ammersee, Germany). Each sample was run in triplicate by scanning 11
207 cell positions under the following settings: Focus: autofocus; Frame rate: 30; Camera
208 sensitivity for all samples: 70 for scatter, 87 for Di8; Shutter: 100; Scattering Intensity:
209 detected automatically; Cell temperature: 25 ºC. The videos were analyzed with the
210 built-in ZetaView® Software 8.05.12 SP2 with specific analysis parameters: Maximum
211 area: 1000, Minimum area 10, Minimum brightness: 20. Hardware: embedded laser: 488
212 and 520 nm. Di-8-ANEPPS, final concentration 2 μM, (Thermo Fisher Scientific) was

213 used to stain HMEVs as described (51); camera: CMOS. EV concentration (EV
214 particles/mL) was calculated by accounting for dilution factors.
215
216 **2.4.3 Morphological characterization of exosomes by negative transmission**
217 **electron microscopy (TEM)**
218 Electron microscopy was performed at the Multiscale Microscopy Core, an Oregon
219 Health & Science University Shared Resource facility. Briefly, EV preparations were
220 fixed in s 4% paraformaldehyde (PFA) solution (Thermo Scientific). Five microliters of
221 fixed EVs were deposited onto glow discharged (60 secs 15 mA, negative mode) carbon
222 formvar 400 Mesh copper grids (Ted Pella 01822-F) for 3 min, rinsed 30 sec in water,
223 wicked on Whatman filter paper 1, stained for 60 sec in filtered 1.33% (w/v) uranyl
224 acetate in water, wicked and air dried. Samples were imaged at 120 kV on a FEI
225 Tecnai™ Spirit TEM system. Images were acquired using the AMT software interface on
226 a NanoSprint™12S-B CMOS camera system.
227
228 **2.5 Enteroid cultures**
229 **2.5.1 Neonatal human enteroid generation and culture**
230 Tissue collected for enteroid generation was approved under OHSU IRB # 21952.
231 Enteroids were generated from small intestinal tissue isolated from the ileum of a 2-
232 month-old patient born at 39 weeks undergoing surgery for ileal atresia. After collection,
233 tissue was washed in sterile PBS with 1% penicillin/streptomycin and frozen in freezing
234 media (10% FBS; 10% DMSO; Dulbecco's modified Eagle medium/F12). Tissue was
235 rapidly thawed in a 37 ºC water bath and then washed three times in sterile PBS with
236 10% FBS. Luminal pinch biopsies were collected. The biopsies were minced in sterile
237 PBS with 10% FBS using sterile scissors and spun at 300 x g for 3 min at 4 ºC. The

238 pellet was resuspended in 500 µl of “working solution”: Liberase™ TH 0.1 WU/mL
239 (Sigma, St. Louis, MO, USA); DNAse1 50 U/mL (Roche, Indianapolis, IN, USA); Hank’s
240 balanced salt solution (HBSS) and incubated in a Thermomixer at 800rpm for 10 min at
241 37 ºC. During the incubation, a 100 µm strainer was washed with 8 mL of 4% bovine
242 serum albumin (BSA) in HBSS to prevent cells from sticking to the filter. The tissue was
243 pelleted at 300 x g for 3 min at 4 ºC and the supernatant was passed through the
244 prepared 100 µm strainer. The remaining tissue fragments were resuspended in another
245 500 µl of working solution and mixed in the Thermomixer® at 800 rpm for 10 min at 37
246 ºC. After incubation, the sample was passed through a P1000 pipettor tip 10 times and
247 spun down at 300 x g for 3 min at 4 ºC. The supernatant was filtered through the same
248 100 µm strainer and the tissue pellet was resuspended in 500 µl of working solution and
249 mixed in the Thermomixer at 800 rpm for 10 min at 37 ºC. The remaining tissue was
250 passed through a P200 pipettor tip on the end of a P1000 tip 10 times. Once the tissue
251 was small enough, the slurry was filtered through the same 100 µm strainer. The filtered
252 cells were pelleted at 500 x g for 5 min at 4 ºC. The pellet was resuspended in 500 µl of
253 4% BSA in HBSS and counted using Trypan Blue staining (Gibco) and a Countess cell
254 counter (Invitrogen). The cells were seeded at a density of up to 10^5 live cells per 30 µl
255 Matrigel (Corning, Corning, NY, USA) dome (80% Matrigel). After the Matrigel solidified
256 at 37 ºC, Human Intesticult™ (StemCell Technologies, Cambridge, MA, USA) with
257 Primocin® (20 µl of a 500X stock, InvivoGen, San Diego, CA, USA) was overlaid.
258 Primocin® was discontinued after the second passage and the enteroids were
259 supplemented with Anti/Anti (Gibco). Enteroids were maintained and expanded in
260 Matrigel patties in the “basal out” orientation.

261

262 **2.5.2 Apical-out enteroids**

263 To access the apical/luminal surface of the human enteroids, we reversed enteroid
264 polarity using the technique described previously (52, 53). Briefly, 1 mL of ice-cold cell
265 recovery solution (Corning) was added directly to the exposed Matrigel dome to break
266 up the Matrigel patty. The enteroid/Matrigel mixture was transferred to a 15 mL conical
267 tube and rotated at 4 ºC for 1 hr. The enteroids were then pelleted at 300 x g for 3 min at
268 4 ºC and washed once with advanced DMEM/F-12 basal media (Gibco). The enteroid
269 pellet was resuspended in the desired volume of IntestiCult complete medium (Stemcell
270 Technologies) and cultures were maintained in a 24-well ultra-low-attachment plate for
271 48 hours at 37 ºC in a 5% CO_2 incubator.

272

273 **2.6 RNA isolation and qRT-PCR**

274 To isolate RNA from enteroids, the media was removed and cell recovery solution was
275 added to remove Matrigel. The enteroids were pelleted, washed with PBS, and pelleted
276 again. RNA was isolated using GeneJET™ RNA Purification Kit (Thermo Scientific) or
277 RNAqueous™-Micro Total RNA Isolation Kit (Invitrogen). High-capacity cDNA Reverse
278 Transcription Kit (Applied Biosystems™, Thermo Fisher) was used to synthesize cDNA.

279 The following primer-probe sets were used: leucine-rich repeat containing G
280 protein (*LGR5*, Hs00969422_m1), marker of proliferation Ki-67 (*Ki67*, Hs00606991_m1),
281 proliferating cell nuclear antigen (*PCNA*, Hs00696862_m1), polycomb complex protein
282 BMI1 proto-oncogene (*BMI1*, Hs00180411_m1), DEF6 guanine nucleotide exchange
283 factor (*DEF6*, Hs00427001_m1), intracellular adhesion molecule 2 (*ICAM2*,
284 Hs00609563), bestrophin 4 (*BEST4*, Hs00396114_m1), sucrase-isomaltase (*SI*,
285 Hs00356112_m1), chromogranin A (*CHGA*, Hs00900370_m1), mucin 2 (*MUC2*,
286 Hs00159374_m1).

287

288 **2.7 EV labeling with CMTPX**

289 Five hundred microliters dHMEV fractions were stained with 4 µL 1 mM CMTPX dye
290 (Invitrogen) in a 37º C water bath for 1 hour in the dark. The excess dye was removed
291 using Amicon® Ultra-0.5 100kDa MWCO centrifugal filter (Millipore, Burlington, MA,
292 USA), and fractions were concentrated to the desired volume for uptake experiments.

293

294 **2.8 Uptake of dHMEVs by human neonatal enteroids**

295 CMTPX-labeled dHMEVs (40 µL) were added to apical-out enteroids and incubated for
296 1.5 hours in the following conditions: at 37 ºC with or without 200 µM Dynasore (Abcam),
297 or at 4 ºC. After dHMEV treatment, enteroids were pelleted and washed one time with
298 1X PBS and fixed in 4% (w/v) PFA (Fisher Scientific) for 15 min at room temperature.
299 Fixed enteroids were pelleted and then incubated with 0.1% Triton-X for 15 min at room
300 temperature, pelleted, and incubated with 165 nM Phalloidin (Fisher Scientific) for 40
301 min, followed by 600 nM DAPI (Thermo Fisher) for 10 min at RT in the dark. Enteroids
302 were pelleted and mounted using Molecular Probes Prolong™ Gold Antifade Mountant
303 (Thermo Fisher) and sealed with CoverGrip Coverslip sealant (Biotium, Fremont, CA,
304 USA).

305

306 **2.9 Confocal microscopy and image processing**

307 dHMEV uptake was observed using a Zeiss LSM980 confocal laser microscope with a
308 20X NA objective (Carl Zeiss Microscopy GmbH), and lasers 405 nm (DAPI), 488
309 (Phalloidin), and 555 nm (CMTPX). Images were acquired using 4X line averaging. Z
310 stacks were taken through the whole enteroid (36.33 - 77.6µm). Images were processed
311 using ZEN™ v2.5 Blue software (Carl Zeiss Microimaging GmbH). All images were
312 acquired and processed using identical intensity settings unless noted. CMTPX uptake

313 was quantified using ImageJ and images taken with a Keyence BZ-X800 (Keyence,
314 Itasca, IL) using a 2X objective, 1.40 NA.

315 **2.10 Immunostaining**

316 The image with immunostaining for BTN1A1 is from the Human Protein Atlas (54, 55).
317 Lactating human mammary gland tissue was stained for BTN1A1 using Atlas Antibodies
318 Cat#HPA011126, RRID: AB_1845491; 0.1275 mg/mL; Rabbit pAb (55).
319

320 **2.11 Statistical analyses**

321 Data were analyzed with GraphPad Prism® 9 (GraphPad Software, San Diego, USA).
322 Diagrams are presented either as mean ± SEM and symbols represent biological
323 replicates, either individual patient samples or enteroid passages. For the HMEV uptake
324 experiment, symbols represent individual enteroids from a single experiment.
325

326 **3. RESULTS**

327 This study utilized raw and pasteurized human milk, as well as milk digesta (neonatal
328 intestinal contents) samples to examine whether HMEVs reach the neonatal intestine in
329 vivo to be absorbed by IECs.

330 **3.1 A pipeline to isolate HMEVs and dHMEVs from small sample volumes**

331 Human milk (HM) is a complex and heterogeneous biological fluid containing, numerous
332 proteins (including highly abundant casein and immunoglobulins), sugars, emulsified fat
333 globules, small molecules, electrolytes, and EVs (1). Neonatal digesta is also a
334 heterogenous biofluid containing a mixture of fed HM, stomach, and digestive
335 secretions.

336 Isolating EVs from heterogeneous biofluids is challenging, especially when
337 starting volumes are limited and relatively high purity is desired. We adapted the

338 published protocol from Mukhopadhya et al (46) for 1 mL sample volumes followed by
339 bottom-up, rate zone iodixanol density gradient centrifugation to isolate largely pure EVs
340 from HM and neonatal digesta samples (**Figure 1a and b**).

341 **3.2 Pipeline effectively isolates raw and pasteurized HMEVs**

342 We validated our pipeline using raw human milk (RHM) and pasteurized donor human
343 milk (PDHM), respectively (**Table 1**). PDHM from the NW Mother's Milk Bank Batch A
344 was used for **Figure 2.** RHM-derived EVs were enriched in fractions (F)2 and 3, and
345 PDHM-derived EVs were enriched in fraction 3 (**Figure 2**). Negative transmission
346 electron microscopy (TEM) illustrated the enrichment of classic cup-shaped-EV
347 structures ~ 100 – 200 nm in F2 -F3 of RHM and F3 from PDHM (**Figure 2a**).
348 Nanoparticle tracking analysis (NTA) using the lipid membrane dye Di-8-ANEPPS
349 showed that F2-3 RHM and F3 PDHM were enriched for ~ 200 nm-sized particles
350 consistent with TEM data (**Figure 2b**). Based on NTA measurements of F2 and F3 for
351 RHM and F3 of PDHM, HMEV size was not affected by pasteurization, (207.06 ± 7.86
352 nm and 209.68 ± 18.93 nm, n=3 RHM and PDHM, respectively).
353 Western blotting of EV proteins followed the MISEV2018 guidelines (13) to
354 confirm EV enrichment and purity based on the presence and absence of indicated
355 marker proteins. F2 and F3 isolated from RHM (**Figure 2c**) and F3 isolated from PDHM
356 (**Figure 2d)** were enriched for transmembrane proteins CD9, CD63, and CD81.
357 Cytosolic proteins TSG101 and FLOT1 were recovered within RHM EVs, but absent
358 from the pasteurized samples. Our samples lack microvesicle protein ITGB1 (49).
359 Importantly, all of our samples lack the Golgi protein GM130 and are depleted of the
360 whey protein LALBA and highly abundant milk protein CSN2 (**Figure 2c & d**).
361 Additionally, the RHM and PDHM samples also contain BTN1A1, a protein that is
362 prevalent in milk fat globules (56, 57), but also present in HMEVs, as demonstrated by

363 proteomics (58) (**Figure 2c & d**). The western blots support the TEM and NTA data
364 showing EV markers in F2-3 of RHM and only F3 of PDHM. Notably, these data indicate
365 that pasteurization results in the focusing of the EV population into F3 and the depletion
366 or loss of cytosolic proteins, such as TSG101 and FLOT1.
367 Collectively, these data demonstrate that our pipeline effectively and consistently
368 isolates EVs from small volumes of RHM and PDHM.

369 **3.3 Pipeline effectively isolates EVs from neonatal human digesta**

370 Neonatal human digesta was collected by gravity after gastric feeding from oro- or
371 nasoduodenal/jejunal sampling tubes from neonates in the OHSU NICU (**Figure 3a**;
372 **Table 1**). Infants were fed RHM and digesta was isolated from the proximal small
373 intestine (**Figure 3b)**.
374 We isolated and validated the dHMEVs identically to the HMEVs described
375 above. Data for sample (a) is shown in **Figure 3** and samples (b) and (c) are in
376 **Supplemental Figure 1**. Negative TEM shows the greatest enrichment of cup-shaped
377 EV structures in F3 (**Figure 3b; Supplemental Figure 1a**). NTA using Di-8-ANEPPS
378 lipid membrane dye showed that F2-F3 were enriched with 117.73 ± 1.5 and 130.03 ±
379 2.43 nm particles consistent with the TEM data and expected 100-200 nm EV size
380 (**Figure 3c; Supplemental Figure 1b**). Western blotting followed the MISEV2018
381 guidelines (13) to confirm EV enrichment and purity based on the presence or absence
382 of indicated marker proteins. F3 of all three samples was enriched for CD9, while only
383 the more proximal intestinal samples (a) and (b) contained EVs with CD81 (**Figure 3c;**
384 **Supplemental Figure 1c)**. All the samples lacked ITGB1, GM130, and CSN2 (**Figure**
385 **3c; Supplemental Figure 1c)**. BTN1A1 was present in dHMEVs isolated from samples
386 (a) and (c), further supporting their HM origin. In addition to being previously found within
387 HMEVs (58), BTN1A1 is only expressed in the lactating mammary gland (**Figure 3e**)

388 and nowhere else along the digestive tract, including the salivary gland, pancreas,
389 gallbladder, or liver (55).
390 Collectively, these data indicate that pasteurization alters HMEVs and that
391 HMEVs reach the proximal intestine of the neonate.

392 **3.4 Neonatal human enteroids take up dHMEVs**

393 We established that HMEVs reach the neonatal intestinal tract. Next, we asked
394 whether neonatal IECs take up dHMEVs. To test this, we developed a neonatal human
395 enteroid model. Patient-derived enteroids, enteroid-derived monolayers, or gut-on-a-chip
396 systems are emerging models for studying neonatal intestinal physiology and
397 pathophysiology (59-63). Our model is derived from intestinal epithelial stem cells
398 isolated from a 2-month-old patient undergoing surgery for ileal atresia.
399 Our neonatal enteroids were propagated in the basal-out orientation where they
400 grow robustly in Matrigel and the basolateral cell surface faces the culture media (**Figure**
401 **4a**). For these studies, we used the apical-out enteroid model where the enteroids are
402 cultured in suspension in the absence of a basement membrane (52, 59, 62). This leads
403 to polarity reversal, shown by robust phalloidin staining (green) on the outer surface of
404 the enteroid (**Figure 4a**). The apical-out orientation allows for direct access to the apical
405 cell surface, making the culture media effectively equivalent to the intestinal lumen and
406 allowing for manipulation of luminal exposures, such as HMEVs. We first analyzed gene
407 expression for IEC-type specific markers, demonstrating that our apical-out enteroids
408 significantly downregulate markers of proliferation *Ki67* and *LGR5* and upregulate more
409 differentiated markers, such as *CHGA* gene expression relative to basal-out enteroids
410 (**Figure 4b**), which are generally more proliferative (52). Notably, our neonatal enteroids
411 lack Paneth cells (*DEF6*) at baseline, consistent with published findings (64), and down-

412 regulate *BEST4* mRNA. This suggests that our apical-out enteroids represent a more
413 differentiated and less proliferative intestinal epithelium.

414 Once established and validated, we asked whether neonatal enteroids readily
415 take up dHMEVs. Since our dHMEVs are isolated from patient samples, we are unable
416 to label and track using fusion proteins, or fluorescent tags (32, 65). Instead, we
417 developed a novel method for labeling the dHMEVs using CMTPX dye (**Figure 4c**). This
418 dye is nonfluorescent initially but readily permeates the EV lipid bilayer where it is then
419 converted to a fluorescent derivative by glutathione S transferase and retained within the
420 EV. This is important for demonstrating the specificity of EV uptake. We observed the
421 highest level of CMTPX staining in fraction 3 (F3) consistent with TEM, NTA, and
422 western blot data showing the highest number of dHMEVs in F3 (**Figure 4d**).

423 All images were acquired using identical microscope settings. Representative
424 images are shown in (**Figure 4e**). dHMEV uptake was quantified using ImageJ (**Figure**
425 **4f**). At 37ºC we observe robust uptake of CMTPX-labeled dHMEVs by neonatal human
426 enteroids as indicated by a strong red signal. The specificity of the labeling and the
427 uptake were confirmed using a dynamin-2 inhibitor (Dynasore) to block clathrin and
428 caveolin-dependent endocytosis and by performing experiments at 4ºC to block all forms
429 of energy-dependent endocytosis (32, 65-68). Collectively, our results indicate that
430 neonatal human enteroids rapidly take up dHMEVs primarily via energy-mediated
431 endocytic processes, while a smaller proportion of dHMEVs are taken up in the
432 presence of dynamin-2 inhibition. Incubation at 4ºC inhibits nearly all uptake. Further,
433 the data indicate that our labeling is specific and that our samples contain low to
434 negligible levels of unincorporated CMTPX, as free dye would show up as robust
435 labeling via diffusion in the Dynasore + 37 ºC or 4 ºC samples.

436 **4. DISCUSSION**

437 HMEVs are emerging therapeutics and drug delivery vehicles (69-76). Cell
438 culture and animal model studies indicate that undigested, unmodified HMEVs may
439 affect intestinal epithelial biology (15, 19, 23), and limit damage from necrotizing
440 enterocolitis (16, 17, 20-22). Further studies indicate that HMEVs survive in vitro
441 simulated digestion (15, 24, 25), may transit through an animal's digestive tract to
442 transfer cargo or affect other organs, including the brain (15, 28), and/or enhance
443 cognitive performance (29). However, whether these nano-sized information carriers
444 survive to reach the human intestine remained an open question. To address this
445 knowledge gap, we obtained in vivo digested milk samples and optimized an isolation
446 protocol capable of isolating HMEVs from small sample volumes.

447 Isolating EVs from HM is challenging due to protein complexes, such as casein
448 micelles, immunoglobulins, and lipoproteins that can entrap HMEVs, mask less
449 abundant proteins, and interfere with downstream analyses, such as western blotting or
450 mass spectrometry (77). Protein complexes can also mimic the appearance of EVs in
451 NTA. To circumvent these pitfalls, it is common to perform HMEV isolations on large
452 starting volumes, which allow for multiple processing steps to enrich for EVs and remove
453 other bioactive factors that may complicate data interpretation (15, 17, 18, 46, 78, 79).
454 This can be prohibitive if sample volumes are limited (≤ 2mL). In such cases, some
455 published studies use precipitation-based methods, such as ExoQuick® and ExoEasy®
456 (80-82). Although these methods are efficient, they can result in co-isolation of non-EV
457 proteins (83-86). Additionally, EV fractions obtained from ExoQuick® may contain traces
458 of biopolymers that can interfere with mass spectrometry (87).

459 Herein we optimized an isolation pipeline developed for large volumes of milk
460 (46) for use with a 1 mL starting volume of HM or digesta. This method utilizes a
461 combination of acetic acid precipitation and density gradient ultracentrifugation to

462 achieve relatively high yield and relatively high purity HMEVs. We validated our
463 methodology using RHM and PDHM. Our RHM samples were consistently enriched for a
464 combination of tetraspanins CD9, CD63, and CD81 and intravesicular markers FLOT1
465 and TSG101 (13) and de-enriched for microvesicle marker ITGB1 (49), Golgi marker
466 GM130 (13), and milk-specific proteins CSN2 and LALBA (88). Notably, samples were
467 also enriched for BTN1A1. BTN1A1 is exclusively expressed in lactating mammary
468 glands (55) and previously detected in HMEVs by mass spectroscopy (58), suggesting
469 that it may be a good HMEV marker.

470 To further validate our isolation pipeline, we compared raw HMEVs with those
471 isolated from PDHM. Pasteurization heats milk to 60° C for 30 minutes to reduce
472 bacterial load (pathogenic and nonpathogenic) and is currently the standard method of
473 HM processing to ensure safety (89). Pasteurization, however, damages, destroys or
474 alters many bioactive factors found in milk (90). This is consistent with our findings. We
475 observed that pasteurization resulted in a depletion of tetraspanin proteins, a loss of
476 cytoplasmic EV protein markers (FLOT1, TSG101), and a focusing of the EV population
477 into one fraction (F3) of the density gradient. This is consistent with the published work
478 of others showing that pasteurization reduces CD63 protein within HM (91) and bovine
479 milk EVs (92). Notably, our raw and pasteurized samples are not matched, limiting our
480 ability to draw firm conclusions about the effects of pasteurization on EV size or number.
481 Previously published reports indicate that these variables are unchanged (91). Our data
482 add to a growing body of evidence demonstrating that pasteurization damages or
483 destroys some populations of HMEVs (91-93).

484 Our isolation pipeline also effectively isolated HMEVs from neonatal digesta,
485 enabling us to demonstrate for the first time that a proportion of HMEVs survive to reach
486 the proximal intestine of neonates. Our data indicate that the number of HMEVs and the
487 level of HMEV protein varies across patient samples based on our ability to detect EV

488 protein markers and the lactating mammary gland-specific protein BTN1A1 (55). These
489 differences could be due to several factors. Our samples are from infants of similar
490 gestational age, so this is unlikely to explain the observed differences. All samples were
491 frozen before processing, which could impact EV yield and result in some cellular EV
492 contamination (94). However, we believe this was minimal as cellular markers, such as
493 GM130 are absent in our samples. While this is a limitation, we do not believe that this
494 accounts for observed differences, as sample (a) was frozen the longest before
495 processing.

496 The observed variability could be due to inherent differences in the number of
497 HMEVs in the fed human milk. Second, the samples were taken from different regions
498 along the proximal small intestine, which could also influence yield. We observed that
499 the amount of BTN1A1 detected may be related to the proximity of the sample location
500 to the stomach, for example sample (a), contains the highest level of BTN1A1. These
501 regional or sample differences could be due to a combination of differing levels of
502 degradation, dilution, or uptake experienced by the HMEVs.

503 In vitro-simulated digestion studies suggest that EVs can survive low pH and the
504 presence of some digestive enzymes (15, 24, 25), supporting our findings that some
505 HMEVs can survive proximal gastrointestinal digestion. However, this does not account
506 for the observed distinct reduction in HMEV abundance in the proximal intestine. It may
507 be that the in vivo environment of the infant intestine can alter or destroy more HMEVs
508 than previously appreciated. In vitro digestion models also cannot account for possible
509 dilution or HMEV uptake.

510 Previous work from the Dallas lab indicates that intestinal secretions result in
511 approximately 1.3-fold dilution of digesta in the proximal intestine relative to the input
512 (95), indicating that the observed loss of dHMEVs could be partly due to dilution from
513 digestive fluids. Our uptake data indicate relatively rapid dHMEV uptake, suggesting that

514 this might be the most important contributing factor to reduced HMEV number within the
515 neonatal small intestine. Further research will be needed to fully address each of these
516 possibilities.

517 Once we isolated dHMEVs, we next asked whether they were taken up by non-
518 transformed, primary neonatal IECs. To do this, we used a neonatal enteroid (intestinal
519 organoid) model for dHMEV uptake. These enteroids grow rapidly and express expected
520 markers of proliferation in the basal-out state. We utilized published protocols (52, 62) to
521 induce polarity reversal in the enteroids allowing direct access to the apical surface from
522 the culture media. We confirmed the apical-out orientation with phalloidin-staining and
523 gene expression showing a significant down-regulation in proliferative markers,
524 consistent with published studies (52). Notably, markers of absorptive (*SI*) and secretory
525 lineages (*CHGA* and *MUC2*) were elevated, but only differences in *CHGA* were
526 statistically significant, suggesting some variability in the cell lineages present within the
527 apical-out enteroids.

528 We then used CMTPX dye to track dHMEVs ex vivo. Nonfluorescent CMTPX
529 freely diffuses into HMEV double-layered membranes. Once inside, it undergoes a
530 chemical transformation mediated by glutathione-S transferase (GST) (96) rendering it
531 fluorescent and trapping it within the EV. This allows for extra-EV CMTPX to be washed
532 away using chromatography column treatment. Therefore, CMTPX specifically labels
533 isolated EVs and avoids non-specific labeling of cellular or organelle membranes often
534 seen with lipophilic dyes, such as PKH26 (red), PKH27 (green), and C5-maleimide-
535 Alexa633 (96, 97). We observed minimal labeling when endocytosis was inhibited
536 chemically and when all uptake mechanisms were limited by cold temperatures,
537 suggesting that our labeling method is specific and indicates minimal signal from passive
538 dye diffusion. This indicates that CMTPX may be a superior non-genetic method for
539 labeling and tracking EVs.

540 Our data suggest that dHMEVs are rapidly taken up by neonatal enteroids in a
541 process that depends in part on dynamin-mediated endocytosis. This is consistent with
542 the work of others demonstrating that bovine milk EVs are transported via endocytosis
543 into endothelial cells (66) or transformed Caco2 or IEC6 cells (68). In our study, uptake
544 was further significantly decreased by incubation at 4°C, suggesting that other
545 mechanisms may also be involved in dHMEV uptake within the intestine. These could
546 include lipid raft/caveolae-mediated endocytosis (98), phagocytosis, and/or
547 micropinocytosis (99). Importantly, our studies establish a relevant system for performing
548 functional studies and build on published work in immortalized cell lines (24, 25) to show
549 that non-transformed neonatal enteroids readily absorb dHMEVs.
550 Collectively, this study demonstrates that a proportion of HMEVs can survive
551 neonatal digestion to reach the proximal small intestine. These dHMEVs can then be
552 rapidly absorbed ex vivo by neonatal IECs in a process that is partially dependent on
553 dynamin-mediated endocytosis. This study provides a modified protocol for use with
554 small sample volumes and lays the foundation for future, in-depth work investigating the
555 effects of donor human milk processing and gastrointestinal digestion on HMEV
556 structure and contents and how dHMEVs interact with and are taken by the neonatal
557 intestinal epithelium.
558
559 **FIGURE LEGENDS**
560 **Figure 1. Human milk (HM) and neonatal digested human milk extracellular vesicle**
561 **(dHMEV) isolation pipeline.** (A) Samples were quickly thawed in a 37 ºC water bath
562 and used immediately (44, 45). One milliliter of whole HM was used for each isolation.
563 Samples were centrifuged at 6,000 x g for 10 min at 4 ºC to remove cream and large cell
564 debris (46). The supernatant was carefully collected and centrifuged again at 2,000 x g
565 for 20 min at 4 ºC to further remove any fat globules and/or smaller cell debris. This

566 supernatant was then passed through Whatman™ Grade 1 filter paper (diameter
567 42.5mm) using a glass funnel before isoelectric casein precipitation. Acetic acid (1 and
568 10 N) was used to adjust the pH of the supernatant to 4.6 using a portable pH meter.
569 pH-adjusted samples were incubated at room temperature for 10 min. Casein was
570 pelleted by centrifugation at 5,000 x g for 30 min at 4 ºC. The supernatant was collected
571 and passed sequentially through Whatman™ Grade 1 filter paper (diameter 42.5 mm)
572 using a glass funnel, a 0.45 µm syringe filter, and a 0.22 µm syringe filter for further
573 removal of casein. (B) Bottom-up density gradient ultracentrifugation was performed
574 using iodixanol gradient (47). A 45% (w/v) bottom layer was made by diluting OptiPrep™
575 solution with clear HM or digesta (2.25 mL OptiPrep™ + 0.75 mL sample = 3 mL) into a
576 5 mL open-top thin wall ultra-clear tube. The discontinuous gradient with 40% (w/v), 30%
577 (w/v), 20% (w/v), and 10% (w/v) solutions of iodixanol (diluted with sterile, 0.1 µm-filtered
578 PBS) were carefully layered on top, drop by drop. Samples were spun in an
579 ultracentrifuge at 37,400 rpm for 24 hrs at 4 ºC with zero acceleration and deceleration.
580 After ultracentrifugation, 500 µL fractions were carefully collected into individual protein
581 LoBind tubes from top to bottom using a P1000 pipettor without disrupting the layers.
582 The fractions were used immediately for downstream analysis.
583
584 **Figure 2. Pipeline effectively isolates human milk extracellular vesicles (HMEVs)**
585 **from raw (RHM) and pasteurized donor human milk (PDHM).** All data shown are from
586 the same RHM or PDHM sample isolated using the pipeline in Figure 1. (A)
587 Transmission electron micrographs of fractions (F)2 and 3 from RHM and PDHM.
588 Images represent data collected across n=3 biological replicates obtained from three
589 different donors and three different donor human milk sources (Table 1). Scale bar =
590 100nm. (B) Nanoparticle tracking analysis (NTA) was performed on RHM and PDHM F2-
591 5. F1 was below the level of detection. Data represent the average of triplicate runs for

592 each fraction and data is smoothed using Graphpad Prism v9. Size data represents the
593 average median size across triplicate runs. (C) Western blotting assessed the protein
594 profile of isolated HMEVs. Fifteen micrograms of SW480 (colorectal cancer cells), MCF7
595 (breast cancer cells) whole cell lysates (WCL), and whole milk were loaded as positive
596 controls. Twenty microliters of unconcentrated fractions (F) 1-5 of RHM (C) and PDHM
597 (D) were run on a 4-12% Bis-Tris gel, transferred to a PVDF membrane, and probed
598 according to MISEV 2018 guidelines, including controls for common proteins found in
599 human milk (BTN1A1, LALBA, CSN2). Each blot represents triplicate experiments
600 performed on three biological replicates of RHM and PDHM. Data shown are from
601 multiple blots run using the same samples.
602
603 **Figure 3. Pipeline effectively isolates human milk extracellular vesicles from**
604 **neonatal human digesta (dHMEVs).** (A) Neonatal human digesta was collected from
605 infants in the NICU after obtaining parental informed consent. Inclusion criteria included
606 infants already admitted to the NICU, greater than 26 weeks corrected gestational age
607 with an indwelling nasogastric or orogastric feeding tube who were tolerating full enteral
608 feeding volumes. Infants were excluded from the study if they had anatomic or functional
609 gastrointestinal disorders, were medically unstable, were non-viable, or had disorders
610 that would be expected to affect normal digestion. Before feeding, a nasal tube was
611 placed into the proximal small intestine. Feeds were delivered via a gastric tube over 30
612 min or less. Data are from three patients with sampling tubes placed along the
613 duodenum (a, b, c) as shown. (B) Transmission electron micrographs of fractions (F)1 –
614 5 of neonatal digesta collected from patient a. Scale bar = 100nm. (C) Nanoparticle
615 tracking analysis (NTA) performed on neonatal digesta F1-5 isolated from patient a.
616 Data represent the average of triplicate runs for each fraction and data is smoothed
617 using GraphPad Prism v9. Size data represents the average median size across

618 triplicate runs. (D) Western blotting assessed the protein profile of isolated EVs. Fifteen
619 micrograms of SW480 (colorectal cancer cells) and MCF7 (breast cancer cells) whole
620 cell lysates (WCL) were loaded as positive controls. Each fraction was concentrated
621 over an Amicon® concentration column (100kDa MWCO) to allow for loading of the
622 entire fraction volume in the gel; therefore, the data shown represent all the proteins in
623 the fraction from a 1 mL digesta sample. Samples were loaded on a 4-12% Bis-Tris gel,
624 transferred to a PVDF membrane, and probed according to MISEV 2018 guidelines,
625 including controls for common proteins found in human milk (BTN1A1, LALBA, CSN2).
626 LALBA and CSN2 were not detected. Data is not shown as the blot was reprobed after
627 CD9 and shows only the CD9 signal. (E) Immunostaining for BTN1A1 in lactating
628 mammary gland. Image provided courtesy of Human Protein Atlas (54, 55).
629
630 **Figure 4. Neonatal human enteroids take up neonatal digested human milk**
631 **extracellular vesicles (dHMEVs) primarily by dynamin-mediated endocytosis.** (A)
632 Neonatal human enteroids were cultured in Matrigel basement membrane where the
633 basal cell surface faces the media (basal-out) before removing the basement membrane
634 to induce polarity reversal to the “apical-out” orientation for all experiments. DAPI (blue)
635 stains nuclei and phalloidin (green) stains F-actin. Scale bar = 20 μm. (B) Polarity
636 reversal and the apical-out orientation down-regulated expression of *LGR5* and *KI67*
637 relative to basal-out controls. *BEST4* was down-regulated, whereas *CHGA* was
638 increased across passages. Each dot represents a separate passage (biological
639 replicate). Gene expression values are the average of triplicates for each gene within
640 each biological replicate and are normalized to the housekeeping gene *RPLP0*. Data are
641 expressed at Log2-fold change and error bars represent the standard error of the mean
642 (SEM). *p<0.05 was considered statistically significant. (C) dHMEVs were isolated from
643 samples a and c and stained with 10 μM CMTPX dye in a 37 ºC water bath for 1 hour in

644 the dark. (D) The excess dye was removed using Amicon® Ultra-0.5 10 kDa MWCO
645 centrifugal filters and fractions were concentrated to the desired volume for uptake
646 experiments. Apical-out enteroids were treated with CMTPX-stained EVs for 90 minutes
647 at 37 ºC in the presence or absence of the endocytosis inhibitor Dynasore or at 4 ºC.
648 The "No EV" control consisted of PBS incubated with CMTPX dye and filtered through
649 an Amicon® filter. (E) EV uptake was assessed by confocal microscopy on fixed whole-
650 mount enteroids. DAPI (blue) marks nuclei. Phalloidin (Cy2-green) marks F-actin.
651 CMTPX staining is shown in Cy3-red. Scale bar = 20 µm. Data represent a single
652 experiment using a pool of dHMEVs from patients a and c. Images are representative of
653 enteroids imaged across 4 slides for each treatment group. Images were acquired and
654 processed using identical microscope settings. Notably, the Cy2 intensity for the
655 phalloidin staining in the xz.yz projection image for the 4ºC treatment was increased 3-
656 fold to enable visualization of the cell surface. All other channel intensities are matched.
657 (F) CMTPX-labeled dHMEV uptake was quantified using images captured with a 2X
658 objective on a Keyence BZ-X800 microscope. Staining intensity within each enteroid
659 was determined using ImageJ and normalized to the enteroid area. Data represent
660 individual enteroids across 4 slides in each treatment group from a single experiment.
661 The inset shows box and whisker plots of the same data. Data was analyzed by one-way
662 ANOVA with Dunn's test for multiple comparisons. *$p<0.05$ was considered statistically
663 significant.
664

665 **AUTHOR CONTRIBUTIONS**

666 **Conceptualization**: Sarah F. Andres, Brian Scottoline

667 **Sample acquisition and patient data management:** Brian Scottoline, Amy Olyaei

668 Molly Aloia

669 **Methodology**: Yang Zhang, Madeline Kuhn, Randall J. Armstrong, Sarah F. Andres

670 **Data acquisition:** Yang Zhang, Madeline Kuhn, Claire Yung

671 **Funding acquisition**: Sarah F. Andres, Brian Scottoline

672 **Writing**: Sarah F. Andres, Yang Zhang, Claire Yung, Madeline Kuhn

673 **Review & editing**: Sarah F. Andres, Brian Scottoline

674 **Approved manuscript:** all authors

675 **ACKNOWLEDGEMENTS**

676 SFA is supported by the National Institutes of Health (NIH) grant K01DK129401 and

677 grants from the Collins Medical Trust, Medical Research Foundation, and OHSU

678 Exploratory Research Seed Grant. BS is supported by the Gerber Foundation #21-9161,

679 a grant from Evolve BioSystems, and NIH grant R01HD097367. The authors would like

680 to thank Dr. Pepper Schedin for sharing the MCF7 cell line. The authors kindly

681 acknowledge Steven Adamou, Erin Stempinski, and Dr. Claudia Lopez from the OHSU

682 Multiscale Microscopy Core for their technical expertise and assistance with the negative

683 staining and electron microscopy. Brian Jenkins, Dr. Felice Kelly, and Dr. Stefanie

684 Kaech Petrie from the OHSU Advanced Light Microscopy Core for their technical

685 expertise and assistance with confocal microscopy.

686 **CONFLICT OF INTERESTS**

687 The authors report no conflict of interest.

688

689

690 **REFERENCES**

691

692 1. Andres SF, Scottoline B, Good M. Shaping infant development from the
693 inside out: Bioactive factors in human milk. Semin Perinatol. 2023;47(1):151690.
694 Epub 2022/12/30. doi: 10.1016/j.semperi.2022.151690. PubMed PMID:
695 36581527; PMCID: PMC9974576.
696 2. Barlow B, Santulli TV, Heird WC, Pitt J, Blanc WA, Schullinger JN. An
697 experimental study of acute neonatal enterocolitis--the importance of breast milk.
698 J Pediatr Surg. 1974;9(5):587-95. Epub 1974/10/01. doi: 10.1016/0022-
699 3468(74)90093-1. PubMed PMID: 4138917.
700 3. Boyd CA, Quigley MA, Brocklehurst P. Donor breast milk versus infant
701 formula for preterm infants: systematic review and meta-analysis. Arch Dis Child
702 Fetal Neonatal Ed. 2007;92(3):F169-75. Epub 2006/03/25. doi:
703 10.1136/adc.2005.089490. PubMed PMID: 16556615; PMCID: PMC2675323.
704 4. Chowning R, Radmacher P, Lewis S, Serke L, Pettit N, Adamkin DH. A
705 retrospective analysis of the effect of human milk on prevention of necrotizing
706 enterocolitis and postnatal growth. J Perinatol. 2016;36(3):221-4. Epub
707 2015/12/04. doi: 10.1038/jp.2015.179. PubMed PMID: 26633147.
708 5. Cortez J, Makker K, Kraemer DF, Neu J, Sharma R, Hudak ML. Maternal
709 milk feedings reduce sepsis, necrotizing enterocolitis and improve outcomes of
710 premature infants. J Perinatol. 2018;38(1):71-4. Epub 2017/10/20. doi:
711 10.1038/jp.2017.149. PubMed PMID: 29048409.
712 6. Good M, Sodhi CP, Egan CE, Afrazi A, Jia H, Yamaguchi Y, Lu P, Branca
713 MF, Ma C, Prindle T, Jr., Mielo S, Pompa A, Hodzic Z, Ozolek JA, Hackam DJ.
714 Breast milk protects against the development of necrotizing enterocolitis through
715 inhibition of Toll-like receptor 4 in the intestinal epithelium via activation of the
716 epidermal growth factor receptor. Mucosal Immunol. 2015;8(5):1166-79. Epub
717 2015/04/23. doi: 10.1038/mi.2015.30. PubMed PMID: 25899687; PMCID:
718 PMC4540669.
719 7. Hair AB, Peluso AM, Hawthorne KM, Perez J, Smith DP, Khan JY,
720 O'Donnell A, Powers RJ, Lee ML, Abrams SA. Beyond Necrotizing Enterocolitis
721 Prevention: Improving Outcomes with an Exclusive Human Milk-Based Diet.
722 Breastfeed Med. 2016;11(2):70-4. Epub 2016/01/21. doi:
723 10.1089/bfm.2015.0134. PubMed PMID: 26789484; PMCID: PMC4782036
724 receive any compensation for this study. M.L.L. is an employee of Prolacta
725 Bioscience. No competing financial interests exist for the remaining authors.
726 8. Meister AL, Doheny KK, Travagli RA. Necrotizing enterocolitis: It's not all
727 in the gut. Exp Biol Med (Maywood). 2020;245(2):85-95. Epub 2019/12/08. doi:
728 10.1177/1535370219891971. PubMed PMID: 31810384; PMCID: PMC7016421.
729 9. Nino DF, Sodhi CP, Hackam DJ. Necrotizing enterocolitis: new insights
730 into pathogenesis and mechanisms. Nat Rev Gastroenterol Hepatol.
731 2016;13(10):590-600. Epub 2016/08/19. doi: 10.1038/nrgastro.2016.119.
732 PubMed PMID: 27534694; PMCID: PMC5124124.
733 10. Quigley M, Embleton ND, McGuire W. Formula versus donor breast milk
734 for feeding preterm or low birth weight infants. Cochrane Database Syst Rev.

2018;6:CD002971. Epub 2018/06/22. doi: 10.1002/14651858.CD002971.pub4. PubMed PMID: 29926476; PMCID: PMC6513381.

11. Belfort MB, Inder TE. Human Milk and Preterm Infant Brain Development: A Narrative Review. Clin Ther. 2022;44(4):612-21. Epub 2022/03/22. doi: 10.1016/j.clinthera.2022.02.011. PubMed PMID: 35307209; PMCID: PMC9133155.

12. Meek JY, Noble L, Section on B. Policy Statement: Breastfeeding and the Use of Human Milk. Pediatrics. 2022;150(1). Epub 2022/08/04. doi: 10.1542/peds.2022-057988. PubMed PMID: 35921640.

13. Thery C, Witwer KW, Aikawa E, Alcaraz MJ, Anderson JD, Andriantsitohaina R, Antoniou A, Arab T, Archer F, Atkin-Smith GK, Ayre DC, Bach JM, Bachurski D, Baharvand H, Balaj L, Baldacchino S, Bauer NN, Baxter AA, Bebawy M, Beckham C, Bedina Zavec A, Benmoussa A, Berardi AC, Bergese P, Bielska E, Blenkiron C, Bobis-Wozowicz S, Boilard E, Boireau W, Bongiovanni A, Borras FE, Bosch S, Boulanger CM, Breakefield X, Breglio AM, Brennan MA, Brigstock DR, Brisson A, Broekman ML, Bromberg JF, Bryl-Gorecka P, Buch S, Buck AH, Burger D, Busatto S, Buschmann D, Bussolati B, Buzas EI, Byrd JB, Camussi G, Carter DR, Caruso S, Chamley LW, Chang YT, Chen C, Chen S, Cheng L, Chin AR, Clayton A, Clerici SP, Cocks A, Cocucci E, Coffey RJ, Cordeiro-da-Silva A, Couch Y, Coumans FA, Coyle B, Crescitelli R, Criado MF, D'Souza-Schorey C, Das S, Datta Chaudhuri A, de Candia P, De Santana EF, De Wever O, Del Portillo HA, Demaret T, Deville S, Devitt A, Dhondt B, Di Vizio D, Dieterich LC, Dolo V, Dominguez Rubio AP, Dominici M, Dourado MR, Driedonks TA, Duarte FV, Duncan HM, Eichenberger RM, Ekstrom K, El Andaloussi S, Elie-Caille C, Erdbrugger U, Falcon-Perez JM, Fatima F, Fish JE, Flores-Bellver M, Forsonits A, Frelet-Barrand A, Fricke F, Fuhrmann G, Gabrielsson S, Gamez-Valero A, Gardiner C, Gartner K, Gaudin R, Gho YS, Giebel B, Gilbert C, Gimona M, Giusti I, Goberdhan DC, Gorgens A, Gorski SM, Greening DW, Gross JC, Gualerzi A, Gupta GN, Gustafson D, Handberg A, Haraszti RA, Harrison P, Hegyesi H, Hendrix A, Hill AF, Hochberg FH, Hoffmann KF, Holder B, Holthofer H, Hosseinkhani B, Hu G, Huang Y, Huber V, Hunt S, Ibrahim AG, Ikezu T, Inal JM, Isin M, Ivanova A, Jackson HK, Jacobsen S, Jay SM, Jayachandran M, Jenster G, Jiang L, Johnson SM, Jones JC, Jong A, Jovanovic-Talisman T, Jung S, Kalluri R, Kano SI, Kaur S, Kawamura Y, Keller ET, Khamari D, Khomyakova E, Khvorova A, Kierulf P, Kim KP, Kislinger T, Klingeborn M, Klinke DJ, 2nd, Kornek M, Kosanovic MM, Kovacs AF, Kramer-Albers EM, Krasemann S, Krause M, Kurochkin IV, Kusuma GD, Kuypers S, Laitinen S, Langevin SM, Languino LR, Lannigan J, Lasser C, Laurent LC, Lavieu G, Lazaro-Ibanez E, Le Lay S, Lee MS, Lee YXF, Lemos DS, Lenassi M, Leszczynska A, Li IT, Liao K, Libregts SF, Ligeti E, Lim R, Lim SK, Line A, Linnemannstons K, Llorente A, Lombard CA, Lorenowicz MJ, Lorincz AM, Lotvall J, Lovett J, Lowry MC, Loyer X, Lu Q, Lukomska B, Lunavat TR, Maas SL, Malhi H, Marcilla A, Mariani J, Mariscal J, Martens-Uzunova ES, Martin-Jaular L, Martinez MC, Martins VR, Mathieu M, Mathivanan S, Maugeri M, McGinnis LK, McVey MJ, Meckes DG, Jr., Meehan KL, Mertens I, Minciacchi VR, Moller A, Moller Jorgensen M, Morales-Kastresana A, Morhayim J, Mullier F, Muraca M,

Musante L, Mussack V, Muth DC, Myburgh KH, Najrana T, Nawaz M, Nazarenko I, Nejsum P, Neri C, Neri T, Nieuwland R, Nimrichter L, Nolan JP, Nolte-'t Hoen EN, Noren Hooten N, O'Driscoll L, O'Grady T, O'Loghlen A, Ochiya T, Olivier M, Ortiz A, Ortiz LA, Osteikoetxea X, Ostergaard O, Ostrowski M, Park J, Pegtel DM, Peinado H, Perut F, Pfaffl MW, Phinney DG, Pieters BC, Pink RC, Pisetsky DS, Pogge von Strandmann E, Polakovicova I, Poon IK, Powell BH, Prada I, Pulliam L, Quesenberry P, Radeghieri A, Raffai RL, Raimondo S, Rak J, Ramirez MI, Raposo G, Rayyan MS, Regev-Rudzki N, Ricklefs FL, Robbins PD, Roberts DD, Rodrigues SC, Rohde E, Rome S, Rouschop KM, Rughetti A, Russell AE, Saa P, Sahoo S, Salas-Huenuleo E, Sanchez C, Saugstad JA, Saul MJ, Schiffelers RM, Schneider R, Schoyen TH, Scott A, Shahaj E, Sharma S, Shatnyeva O, Shekari F, Shelke GV, Shetty AK, Shiba K, Siljander PR, Silva AM, Skowronek A, Snyder OL, 2nd, Soares RP, Sodar BW, Soekmadji C, Sotillo J, Stahl PD, Stoorvogel W, Stott SL, Strasser EF, Swift S, Tahara H, Tewari M, Timms K, Tiwari S, Tixeira R, Tkach M, Toh WS, Tomasini R, Torrecilhas AC, Tosar JP, Toxavidis V, Urbanelli L, Vader P, van Balkom BW, van der Grein SG, Van Deun J, van Herwijnen MJ, Van Keuren-Jensen K, van Niel G, van Royen ME, van Wijnen AJ, Vasconcelos MH, Vechetti IJ, Jr., Veit TD, Vella LJ, Velot E, Verweij FJ, Vestad B, Vinas JL, Visnovitz T, Vukman KV, Wahlgren J, Watson DC, Wauben MH, Weaver A, Webber JP, Weber V, Wehman AM, Weiss DJ, Welsh JA, Wendt S, Wheelock AM, Wiener Z, Witte L, Wolfram J, Xagorari A, Xander P, Xu J, Yan X, Yanez-Mo M, Yin H, Yuana Y, Zappulli V, Zarubova J, Zekas V, Zhang JY, Zhao Z, Zheng L, Zheutlin AR, Zickler AM, Zimmermann P, Zivkovic AM, Zocco D, Zuba-Surma EK. Minimal information for studies of extracellular vesicles 2018 (MISEV2018): a position statement of the International Society for Extracellular Vesicles and update of the MISEV2014 guidelines. J Extracell Vesicles. 2018;7(1):1535750. Epub 2019/01/15. doi: 10.1080/20013078.2018.1535750. PubMed PMID: 30637094; PMCID: PMC6322352.

14. Maghraby MK, Li B, Chi L, Ling C, Benmoussa A, Provost P, Postmus AC, Abdi A, Pierro A, Bourdon C, Bandsma RHJ. Extracellular vesicles isolated from milk can improve gut barrier dysfunction induced by malnutrition. Sci Rep. 2021;11(1):7635. Epub 2021/04/09. doi: 10.1038/s41598-021-86920-w. PubMed PMID: 33828139; PMCID: PMC8026962.

15. Tong L, Zhang S, Liu Q, Huang C, Hao H, Tan MS, Yu X, Lou CKL, Huang R, Zhang Z, Liu T, Gong P, Ng CH, Muthiah M, Pastorin G, Wacker MG, Chen X, Storm G, Lee CN, Zhang L, Yi H, Wang JW. Milk-derived extracellular vesicles protect intestinal barrier integrity in the gut-liver axis. Sci Adv. 2023;9(15):eade5041. Epub 2023/04/13. doi: 10.1126/sciadv.ade5041. PubMed PMID: 37043568; PMCID: PMC10096581.

16. Pisano C, Galley J, Elbahrawy M, Wang Y, Farrell A, Brigstock D, Besner GE. Human Breast Milk-Derived Extracellular Vesicles in the Protection Against Experimental Necrotizing Enterocolitis. J Pediatr Surg. 2020;55(1):54-8. Epub 2019/11/07. doi: 10.1016/j.jpedsurg.2019.09.052. PubMed PMID: 31685268; PMCID: PMC6989376.

17. Miyake H, Lee C, Chusilp S, Bhalla M, Li B, Pitino M, Seo S, O'Connor DL, Pierro A. Human breast milk exosomes attenuate intestinal damage. Pediatr Surg Int. 2020;36(2):155-63. Epub 2019/11/13. doi: 10.1007/s00383-019-04599-7. PubMed PMID: 31713717.
18. Zonneveld MI, van Herwijnen MJC, Fernandez-Gutierrez MM, Giovanazzi A, de Groot AM, Kleinjan M, van Capel TMM, Sijts A, Taams LS, Garssen J, de Jong EC, Kleerebezem M, Nolte-'t Hoen ENM, Redegeld FA, Wauben MHM. Human milk extracellular vesicles target nodes in interconnected signalling pathways that enhance oral epithelial barrier function and dampen immune responses. J Extracell Vesicles. 2021;10(5):e12071. Epub 2021/03/19. doi: 10.1002/jev2.12071. PubMed PMID: 33732416; PMCID: PMC7944547.
19. Wang L, Gao R, Li B, Alganabi M, He W, Shen C, Zhu H, Pierro A. Human breast milk-derived exosomes protect against intestinal ischemia and reperfusion injury in neonatal rats. J Pediatr Surg. 2022;57(7):1264-8. Epub 2022/04/06. doi: 10.1016/j.jpedsurg.2022.02.029. PubMed PMID: 35379491.
20. Dong P, Zhang Y, Yan DY, Wang Y, Xu X, Zhao YC, Xiao TT. Protective Effects of Human Milk-Derived Exosomes on Intestinal Stem Cells Damaged by Oxidative Stress. Cell Transplant. 2020;29:963689720912690. Epub 2020/03/21. doi: 10.1177/0963689720912690. PubMed PMID: 32193954; PMCID: PMC7444213.
21. He S, Liu G, Zhu X. Human breast milk-derived exosomes may help maintain intestinal epithelial barrier integrity. Pediatr Res. 2021;90(2):366-72. Epub 2021/03/19. doi: 10.1038/s41390-021-01449-y. PubMed PMID: 33731816.
22. Gao R, Zhang R, Qian T, Peng X, He W, Zheng S, Cao Y, Pierro A, Shen C. A comparison of exosomes derived from different periods breast milk on protecting against intestinal organoid injury. Pediatr Surg Int. 2019;35(12):1363-8. Epub 2019/10/03. doi: 10.1007/s00383-019-04562-6. PubMed PMID: 31576466.
23. Martin C, Patel M, Williams S, Arora H, Brawner K, Sims B. Human breast milk-derived exosomes attenuate cell death in intestinal epithelial cells. Innate Immun. 2018;24(5):278-84. Epub 2018/07/12. doi: 10.1177/1753425918785715. PubMed PMID: 29991305; PMCID: PMC6830917.
24. Kahn S, Liao Y, Du X, Xu W, Li J, Lonnerdal B. Exosomal MicroRNAs in Milk from Mothers Delivering Preterm Infants Survive in Vitro Digestion and Are Taken Up by Human Intestinal Cells. Mol Nutr Food Res. 2018;62(11):e1701050. Epub 2018/04/13. doi: 10.1002/mnfr.201701050. PubMed PMID: 29644801.
25. Liao Y, Du X, Li J, Lonnerdal B. Human milk exosomes and their microRNAs survive digestion in vitro and are taken up by human intestinal cells. Mol Nutr Food Res. 2017;61(11). Epub 2017/07/09. doi: 10.1002/mnfr.201700082. PubMed PMID: 28688106.
26. Kosaka N, Izumi H, Sekine K, Ochiya T. microRNA as a new immune-regulatory agent in breast milk. Silence. 2010;1(1):7. Epub 2010/03/17. doi: 10.1186/1758-907X-1-7. PubMed PMID: 20226005; PMCID: PMC2847997.
27. Sadri M, Shu J, Kachman SD, Cui J, Zempleni J. Milk exosomes and miRNA cross the placenta and promote embryo survival in mice. Reproduction.

871 2020;160(4):501-9. Epub 2020/07/06. doi: 10.1530/REP-19-0521. PubMed
872 PMID: 32621589.
873 28. Manca S, Upadhyaya B, Mutai E, Desaulniers AT, Cederberg RA, White
874 BR, Zempleni J. Milk exosomes are bioavailable and distinct microRNA cargos
875 have unique tissue distribution patterns. Sci Rep. 2018;8(1):11321. Epub
876 2018/07/29. doi: 10.1038/s41598-018-29780-1. PubMed PMID: 30054561;
877 PMCID: PMC6063888 Agriculture (NIFA), the National Institutes of Health, the
878 Gerber Foundation, the United States Department of Agriculture/Egg Nutrition
879 Center, a grant from the Office of the President of the University of Nebraska, the
880 Nebraska Agricultural Research Division (Hatch Act) and a United States
881 Department of Agriculture multistate group. He has received compensation as a
882 member of the scientific advisory board of PureTech Health, Inc. and has a
883 licensing agreement with the company. He also has consulted for PureTech
884 Health and received compensation. He has submitted a provisional patent
885 application titled Extracellular Vesicles and Methods of Using (62/471,572) to the
886 U.S. Patents and Trademarks Office. Dr White's work has been supported by the
887 Nebraska Agricultural Research Division. The authors declare no potential
888 conflict of interest.
889 29. Zhou F, Ebea P, Mutai E, Wang H, Sukreet S, Navazesh S, Dogan H, Li
890 W, Cui J, Ji P, Ramirez DMO, Zempleni J. Small Extracellular Vesicles in Milk
891 Cross the Blood-Brain Barrier in Murine Cerebral Cortex Endothelial Cells and
892 Promote Dendritic Complexity in the Hippocampus and Brain Function in
893 C57BL/6J Mice. Front Nutr. 2022;9:838543. Epub 2022/05/24. doi:
894 10.3389/fnut.2022.838543. PubMed PMID: 35600828; PMCID: PMC9121399.
895 30. Gonnella PA, Neutra MR. Membrane-bound and fluid-phase
896 macromolecules enter separate prelysosomal compartments in absorptive cells
897 of suckling rat ileum. J Cell Biol. 1984;99(3):909-17. Epub 1984/09/01. doi:
898 10.1083/jcb.99.3.909. PubMed PMID: 6470044; PMCID: PMC2113398.
899 31. Wilson JM, Whitney JA, Neutra MR. Identification of an endosomal
900 antigen specific to absorptive cells of suckling rat ileum. J Cell Biol.
901 1987;105(2):691-703. Epub 1987/08/01. doi: 10.1083/jcb.105.2.691. PubMed
902 PMID: 3305521; PMCID: PMC2114780.
903 32. Bonsergent E, Grisard E, Buchrieser J, Schwartz O, Thery C, Lavieu G.
904 Quantitative characterization of extracellular vesicle uptake and content delivery
905 within mammalian cells. Nat Commun. 2021;12(1):1864. Epub 2021/03/27. doi:
906 10.1038/s41467-021-22126-y. PubMed PMID: 33767144; PMCID: PMC7994380.
907 33. Mulcahy LA, Pink RC, Carter DR. Routes and mechanisms of extracellular
908 vesicle uptake. J Extracell Vesicles. 2014;3. Epub 2014/08/22. doi:
909 10.3402/jev.v3.24641. PubMed PMID: 25143819; PMCID: PMC4122821.
910 34. Betker JL, Angle BM, Graner MW, Anchordoquy TJ. The Potential of
911 Exosomes From Cow Milk for Oral Delivery. J Pharm Sci. 2019;108(4):1496-505.
912 Epub 2018/11/24. doi: 10.1016/j.xphs.2018.11.022. PubMed PMID: 30468828;
913 PMCID: PMC6788294.
914 35. Roerig J, Schiller L, Kalwa H, Hause G, Vissiennon C, Hacker MC, Wolk
915 C, Schulz-Siegmund M. A focus on critical aspects of uptake and transport of
916 milk-derived extracellular vesicles across the Caco-2 intestinal barrier model. Eur

917 J Pharm Biopharm. 2021;166:61-74. Epub 2021/06/03. doi:
918 10.1016/j.ejpb.2021.05.026. PubMed PMID: 34077790.
919 36. Miller ME, Michaylira CZ, Simmons JG, Ney DM, Dahly EM, Heath JK,
920 Lund PK. Suppressor of cytokine signaling-2: a growth hormone-inducible
921 inhibitor of intestinal epithelial cell proliferation. Gastroenterology.
922 2004;127(2):570-81. Epub 2004/08/10. doi: 10.1053/j.gastro.2004.05.016.
923 PubMed PMID: 15300589.
924 37. Andres SF, Simmons JG, Mah AT, Santoro MA, Van Landeghem L, Lund
925 PK. Insulin receptor isoform switching in intestinal stem cells, progenitors,
926 differentiated lineages and tumors: evidence that IR-B limits proliferation. J Cell
927 Sci. 2013;126(Pt 24):5645-56. Epub 2013/10/16. doi: 10.1242/jcs.132985.
928 PubMed PMID: 24127567; PMCID: PMC3860310.
929 38. Chantret I, Barbat A, Dussaulx E, Brattain MG, Zweibaum A. Epithelial
930 polarity, villin expression, and enterocytic differentiation of cultured human colon
931 carcinoma cells: a survey of twenty cell lines. Cancer Res. 1988;48(7):1936-42.
932 Epub 1988/04/01. PubMed PMID: 3349466.
933 39. Pinto M, Robineleon S, Appay MD, Kedinger M, Triadou N, Dussaulx E,
934 Lacroix B, Simonassmann P, Haffen K, Fogh J, Zweibaum A. Enterocyte-Like
935 Differentiation and Polarization of the Human-Colon Carcinoma Cell-Line Caco-2
936 in Culture. Biol Cell. 1983;47(3):323-30. PubMed PMID: ISI:A1983QX96200008.
937 40. Perreault N, Beaulieu JF. Use of the dissociating enzyme thermolysin to
938 generate viable human normal intestinal epithelial cell cultures. Exp Cell Res.
939 1996;224(2):354-64. Epub 1996/05/01. doi: 10.1006/excr.1996.0145. PubMed
940 PMID: 8612712.
941 41. Mahe MM, Aihara E, Schumacher MA, Zavros Y, Montrose MH, Helmrath
942 MA, Sato T, Shroyer NF. Establishment of Gastrointestinal Epithelial Organoids.
943 Curr Protoc Mouse Biol. 2013;3(4):217-40. Epub 2014/08/12. doi:
944 10.1002/9780470942390.mo130179. PubMed PMID: 25105065; PMCID:
945 PMC4120977.
946 42. Sato T, Vries RG, Snippert HJ, van de Wetering M, Barker N, Stange DE,
947 van Es JH, Abo A, Kujala P, Peters PJ, Clevers H. Single Lgr5 stem cells build
948 crypt-villus structures in vitro without a mesenchymal niche. Nature.
949 2009;459(7244):262-5. Epub 2009/03/31. doi: 10.1038/nature07935. PubMed
950 PMID: 19329995.
951 43. Lechuga S, Braga-Neto MB, Naydenov NG, Rieder F, Ivanov AI.
952 Understanding disruption of the gut barrier during inflammation: Should we
953 abandon traditional epithelial cell lines and switch to intestinal organoids? Front
954 Immunol. 2023;14:1108289. Epub 2023/03/07. doi:
955 10.3389/fimmu.2023.1108289. PubMed PMID: 36875103; PMCID:
956 PMC9983034.
957 44. Kenigsberg S, Wyse BA, Librach CL, da Silveira JC. Protocol for Exosome
958 Isolation from Small Volume of Ovarian Follicular Fluid: Evaluation of
959 Ultracentrifugation and Commercial Kits. Methods Mol Biol. 2017;1660:321-41.
960 Epub 2017/08/23. doi: 10.1007/978-1-4939-7253-1_26. PubMed PMID:
961 28828668.

962 45. Trummer A, De Rop C, Tiede A, Ganser A, Eisert R. Recovery and
963 composition of microparticles after snap-freezing depends on thawing
964 temperature. Blood Coagul Fibrinolysis. 2009;20(1):52-6. Epub 2009/01/01. doi:
965 10.1097/MBC.0b013e32831be9c5. PubMed PMID: 20523165.
966 46. Mukhopadhya A, Santoro J, O'Driscoll L. Extracellular vesicle separation
967 from milk and infant milk formula using acid precipitation and ultracentrifugation.
968 STAR Protoc. 2021;2(4):100821. Epub 2021/09/28. doi:
969 10.1016/j.xpro.2021.100821. PubMed PMID: 34568843; PMCID: PMC8449126.
970 47. Greening DW, Xu R, Ji H, Tauro BJ, Simpson RJ. A protocol for exosome
971 isolation and characterization: evaluation of ultracentrifugation, density-gradient
972 separation, and immunoaffinity capture methods. Methods Mol Biol.
973 2015;1295:179-209. Epub 2015/03/31. doi: 10.1007/978-1-4939-2550-6_15.
974 PubMed PMID: 25820723.
975 48. Consortium E-T, Van Deun J, Mestdagh P, Agostinis P, Akay O, Anand S,
976 Anckaert J, Martinez ZA, Baetens T, Beghein E, Bertier L, Berx G, Boere J,
977 Boukouris S, Bremer M, Buschmann D, Byrd JB, Casert C, Cheng L, Cmoch A,
978 Daveloose D, De Smedt E, Demirsoy S, Depoorter V, Dhondt B, Driedonks TA,
979 Dudek A, Elsharawy A, Floris I, Foers AD, Gartner K, Garg AD, Geeurickx E,
980 Gettemans J, Ghazavi F, Giebel B, Kormelink TG, Hancock G, Helsmoortel H,
981 Hill AF, Hyenne V, Kalra H, Kim D, Kowal J, Kraemer S, Leidinger P, Leonelli C,
982 Liang Y, Lippens L, Liu S, Lo Cicero A, Martin S, Mathivanan S, Mathiyalagan P,
983 Matusek T, Milani G, Monguio-Tortajada M, Mus LM, Muth DC, Nemeth A, Nolte-
984 't Hoen EN, O'Driscoll L, Palmulli R, Pfaffl MW, Primdal-Bengtson B, Romano E,
985 Rousseau Q, Sahoo S, Sampaio N, Samuel M, Scicluna B, Soen B, Steels A,
986 Swinnen JV, Takatalo M, Thaminy S, Thery C, Tulkens J, Van Audenhove I, van
987 der Grein S, Van Goethem A, van Herwijnen MJ, Van Niel G, Van Roy N, Van
988 Vliet AR, Vandamme N, Vanhauwaert S, Vergauwen G, Verweij F, Wallaert A,
989 Wauben M, Witwer KW, Zonneveld MI, De Wever O, Vandesompele J, Hendrix
990 A. EV-TRACK: transparent reporting and centralizing knowledge in extracellular
991 vesicle research. Nat Methods. 2017;14(3):228-32. Epub 2017/03/01. doi:
992 10.1038/nmeth.4185. PubMed PMID: 28245209.
993 49. Lotvall J, Hill AF, Hochberg F, Buzas EI, Di Vizio D, Gardiner C, Gho YS,
994 Kurochkin IV, Mathivanan S, Quesenberry P, Sahoo S, Tahara H, Wauben MH,
995 Witwer KW, Thery C. Minimal experimental requirements for definition of
996 extracellular vesicles and their functions: a position statement from the
997 International Society for Extracellular Vesicles. J Extracell Vesicles.
998 2014;3:26913. Epub 2014/12/30. doi: 10.3402/jev.v3.26913. PubMed PMID:
999 25536934; PMCID: PMC4275645.
1000 50. Mehdiani A, Maier A, Pinto A, Barth M, Akhyari P, Lichtenberg A. An
1001 innovative method for exosome quantification and size measurement. J Vis Exp.
1002 2015(95):50974. Epub 2015/02/05. doi: 10.3791/50974. PubMed PMID:
1003 25650897; PMCID: PMC4354536.
1004 51. Kuhn M, Zhang Y, Favate J, Morita M, Blucher A, Das S, Liang S, Preet R,
1005 Parham LR, Williams KN, Molugu S, Armstrong RJ, Zhang W, Yang J, Hamilton
1006 KE, Dixon DA, Mills G, Morgan TK, Shah P, Andres SF. IMP1/IGF2BP1 in
1007 human colorectal cancer extracellular vesicles. Am J Physiol Gastrointest Liver

1008 Physiol. 2022;323(6):G571-G85. Epub 2022/10/05. doi:
1009 10.1152/ajpgi.00121.2022. PubMed PMID: 36194131; PMCID: PMC9678429.
1010 52. Co JY, Margalef-Catala M, Li X, Mah AT, Kuo CJ, Monack DM, Amieva
1011 MR. Controlling Epithelial Polarity: A Human Enteroid Model for Host-Pathogen
1012 Interactions. Cell Rep. 2019;26(9):2509-20 e4. Epub 2019/02/28. doi:
1013 10.1016/j.celrep.2019.01.108. PubMed PMID: 30811997; PMCID: PMC6391775.
1014 53. Stroulios G, Stahl M, Elstone F, Chang W, Louis S, Eaves A, Simmini S,
1015 Conder RK. Culture Methods to Study Apical-Specific Interactions using
1016 Intestinal Organoid Models. J Vis Exp. 2021(169). Epub 2021/04/13. doi:
1017 10.3791/62330. PubMed PMID: 33843928.
1018 54. Uhlen M, Bjorling E, Agaton C, Szigyarto CA, Amini B, Andersen E,
1019 Andersson AC, Angelidou P, Asplund A, Asplund C, Berglund L, Bergstrom K,
1020 Brumer H, Cerjan D, Ekstrom M, Elobeid A, Eriksson C, Fagerberg L, Falk R, Fall
1021 J, Forsberg M, Bjorklund MG, Gumbel K, Halimi A, Hallin I, Hamsten C, Hansson
1022 M, Hedhammar M, Hercules G, Kampf C, Larsson K, Lindskog M, Lodewyckx W,
1023 Lund J, Lundeberg J, Magnusson K, Malm E, Nilsson P, Odling J, Oksvold P,
1024 Olsson I, Oster E, Ottosson J, Paavilainen L, Persson A, Rimini R, Rockberg J,
1025 Runeson M, Sivertsson A, Skollermo A, Steen J, Stenvall M, Sterky F, Stromberg
1026 S, Sundberg M, Tegel H, Tourle S, Wahlund E, Walden A, Wan J, Wernerus H,
1027 Westberg J, Wester K, Wrethagen U, Xu LL, Hober S, Ponten F. A human
1028 protein atlas for normal and cancer tissues based on antibody proteomics. Mol
1029 Cell Proteomics. 2005;4(12):1920-32. Epub 2005/08/30. doi:
1030 10.1074/mcp.M500279-MCP200. PubMed PMID: 16127175.
1031 55. Lactating Breast/BTN1A1/Tissue staining available from
1032 v23.proteinatalas.org [Internet]. Human Protein Atlas. Available from:
1033 https://www.proteinatlas.org/ENSG00000124557-
1034 BTN1A1/tissue/lactating+breast.
1035 56. Lee H, Padhi E, Hasegawa Y, Larke J, Parenti M, Wang A, Hernell O,
1036 Lonnerdal B, Slupsky C. Compositional Dynamics of the Milk Fat Globule and Its
1037 Role in Infant Development. Front Pediatr. 2018;6:313. Epub 2018/11/22. doi:
1038 10.3389/fped.2018.00313. PubMed PMID: 30460213; PMCID: PMC6232911.
1039 57. Robenek H, Hofnagel O, Buers I, Lorkowski S, Schnoor M, Robenek MJ,
1040 Heid H, Troyer D, Severs NJ. Butyrophilin controls milk fat globule secretion.
1041 Proc Natl Acad Sci U S A. 2006;103(27):10385-90. Epub 2006/06/28. doi:
1042 10.1073/pnas.0600795103. PubMed PMID: 16801554; PMCID: PMC1502467.
1043 58. van Herwijnen MJ, Zonneveld MI, Goerdayal S, Nolte-'t Hoen EN,
1044 Garssen J, Stahl B, Maarten Altelaar AF, Redegeld FA, Wauben MH.
1045 Comprehensive Proteomic Analysis of Human Milk-derived Extracellular Vesicles
1046 Unveils a Novel Functional Proteome Distinct from Other Milk Components. Mol
1047 Cell Proteomics. 2016;15(11):3412-23. Epub 2016/11/03. doi:
1048 10.1074/mcp.M116.060426. PubMed PMID: 27601599; PMCID: PMC5098039.
1049 59. Burge K, Wilson A, Chaaban H. In Vitro Apical-Out Enteroid Model of
1050 Necrotizing Enterocolitis. J Vis Exp. 2022(184). Epub 2022/06/28. doi:
1051 10.3791/64003. PubMed PMID: 35758712; PMCID: PMC9682421.
1052 60. Costello CM, Willsey GG, Richards AF, Kim J, Pizzuto MS, Jaconi S,
1053 Benigni F, Corti D, Mantis NJ, March JC. Transcytosis of IgA Attenuates

1054 Salmonella Invasion in Human Enteroids and Intestinal Organoids. Infect Immun.
1055 2022;90(6):e0004122. Epub 2022/05/18. doi: 10.1128/iai.00041-22. PubMed
1056 PMID: 35579465; PMCID: PMC9202428.
1057 61. Lanik WE, Luke CJ, Nolan LS, Gong Q, Frazer LC, Rimer JM, Gale SE,
1058 Luc R, Bidani SS, Sibbald CA, Lewis AN, Mihi B, Agrawal P, Goree M, Maestas
1059 M, Hu E, Peters DG, Good M. Microfluidic device facilitates in vitro modeling of
1060 human neonatal necrotizing enterocolitis-on-a-chip. JCI Insight. 2023;8(8). Epub
1061 2023/03/08. doi: 10.1172/jci.insight.146496. PubMed PMID: 36881475; PMCID:
1062 PMC10243823.
1063 62. Liebe H, Schlegel C, Cai X, Golubkova A, Loerke C, Leiva T, Hunter CJ.
1064 Apical-Out Enteroids as an Innovative Model for Necrotizing Enterocolitis. J Surg
1065 Res. 2023;283:1106-16. Epub 2023/03/15. doi: 10.1016/j.jss.2022.11.048.
1066 PubMed PMID: 36915002; PMCID: PMC10014931.
1067 63. Wilson A, Burge K, Eckert J, Chaaban H. Effect of Hyaluronic Acid 35 kDa
1068 on an In Vitro Model of Preterm Small Intestinal Injury and Healing using
1069 Enteroid-derived Monolayers. J Vis Exp. 2022(185). Epub 2022/08/10. doi:
1070 10.3791/63758. PubMed PMID: 35943893; PMCID: PMC9680908.
1071 64. He GW, Lin L, DeMartino J, Zheng X, Staliarova N, Dayton T, Begthel H,
1072 van de Wetering WJ, Bodewes E, van Zon J, Tans S, Lopez-Iglesias C, Peters
1073 PJ, Wu W, Kotlarz D, Klein C, Margaritis T, Holstege F, Clevers H. Optimized
1074 human intestinal organoid model reveals interleukin-22-dependency of paneth
1075 cell formation. Cell Stem Cell. 2022;29(9):1333-45 e6. Epub 2022/08/25. doi:
1076 10.1016/j.stem.2022.08.002. PubMed PMID: 36002022; PMCID: PMC9438971.
1077 65. Toribio V, Morales S, Lopez-Martin S, Cardenes B, Cabanas C, Yanez-Mo
1078 M. Development of a quantitative method to measure EV uptake. Sci Rep.
1079 2019;9(1):10522. Epub 2019/07/22. doi: 10.1038/s41598-019-47023-9. PubMed
1080 PMID: 31324885; PMCID: PMC6642168.
1081 66. Kusuma RJ, Manca S, Friemel T, Sukreet S, Nguyen C, Zempleni J.
1082 Human vascular endothelial cells transport foreign exosomes from cow's milk by
1083 endocytosis. Am J Physiol Cell Physiol. 2016;310(10):C800-7. Epub 2016/03/18.
1084 doi: 10.1152/ajpcell.00169.2015. PubMed PMID: 26984735; PMCID:
1085 PMC4895447.
1086 67. Weigel PH, Oka JA. Temperature dependence of endocytosis mediated
1087 by the asialoglycoprotein receptor in isolated rat hepatocytes. Evidence for two
1088 potentially rate-limiting steps. J Biol Chem. 1981;256(6):2615-7. Epub
1089 1981/03/25. PubMed PMID: 6259136.
1090 68. Wolf T, Baier SR, Zempleni J. The Intestinal Transport of Bovine Milk
1091 Exosomes Is Mediated by Endocytosis in Human Colon Carcinoma Caco-2 Cells
1092 and Rat Small Intestinal IEC-6 Cells. J Nutr. 2015;145(10):2201-6. Epub
1093 2015/08/14. doi: 10.3945/jn.115.218586. PubMed PMID: 26269243; PMCID:
1094 PMC4580964.
1095 69. Abels ER, Breakefield XO. Introduction to Extracellular Vesicles:
1096 Biogenesis, RNA Cargo Selection, Content, Release, and Uptake. Cell Mol
1097 Neurobiol. 2016;36(3):301-12. Epub 2016/04/08. doi: 10.1007/s10571-016-0366-
1098 z. PubMed PMID: 27053351; PMCID: PMC5546313.

1099 70. Colombo M, Raposo G, Thery C. Biogenesis, secretion, and intercellular
1100 interactions of exosomes and other extracellular vesicles. Annu Rev Cell Dev
1101 Biol. 2014;30:255-89. Epub 2014/10/08. doi: 10.1146/annurev-cellbio-101512-
1102 122326. PubMed PMID: 25288114.
1103 71. Elliott RO, He M. Unlocking the Power of Exosomes for Crossing
1104 Biological Barriers in Drug Delivery. Pharmaceutics. 2021;13(1). Epub
1105 2021/01/23. doi: 10.3390/pharmaceutics13010122. PubMed PMID: 33477972;
1106 PMCID: PMC7835896.
1107 72. S ELA, Mager I, Breakefield XO, Wood MJ. Extracellular vesicles: biology
1108 and emerging therapeutic opportunities. Nat Rev Drug Discov. 2013;12(5):347-
1109 57. Epub 2013/04/16. doi: 10.1038/nrd3978. PubMed PMID: 23584393.
1110 73. Simeone P, Bologna G, Lanuti P, Pierdomenico L, Guagnano MT,
1111 Pieragostino D, Del Boccio P, Vergara D, Marchisio M, Miscia S, Mariani-
1112 Costantini R. Extracellular Vesicles as Signaling Mediators and Disease
1113 Biomarkers across Biological Barriers. Int J Mol Sci. 2020;21(7). Epub
1114 2020/04/09. doi: 10.3390/ijms21072514. PubMed PMID: 32260425; PMCID:
1115 PMC7178048.
1116 74. van Niel G, D'Angelo G, Raposo G. Shedding light on the cell biology of
1117 extracellular vesicles. Nat Rev Mol Cell Biol. 2018;19(4):213-28. Epub
1118 2018/01/18. doi: 10.1038/nrm.2017.125. PubMed PMID: 29339798.
1119 75. Zhong Y, Wang X, Zhao X, Shen J, Wu X, Gao P, Yang P, Chen J, An W.
1120 Multifunctional Milk-Derived Small Extracellular Vesicles and Their Biomedical
1121 Applications. Pharmaceutics. 2023;15(5). Epub 2023/05/27. doi:
1122 10.3390/pharmaceutics15051418. PubMed PMID: 37242660; PMCID:
1123 PMC10223436.
1124 76. Munir J, Ngu A, Wang H, Ramirez DMO, Zempleni J. Review: Milk Small
1125 Extracellular Vesicles for Use in the Delivery of Therapeutics. Pharm Res.
1126 2023;40(4):909-15. Epub 2022/10/06. doi: 10.1007/s11095-022-03404-w.
1127 PubMed PMID: 36198923.
1128 77. Witwer KW, Buzas EI, Bemis LT, Bora A, Lasser C, Lotvall J, Nolte-'t
1129 Hoen EN, Piper MG, Sivaraman S, Skog J, Thery C, Wauben MH, Hochberg F.
1130 Standardization of sample collection, isolation and analysis methods in
1131 extracellular vesicle research. J Extracell Vesicles. 2013;2. Epub 2013/09/07.
1132 doi: 10.3402/jev.v2i0.20360. PubMed PMID: 24009894; PMCID: PMC3760646.
1133 78. Chen W, Chen X, Qian Y, Wang X, Zhou Y, Yan X, Yu B, Yao S, Yu Z,
1134 Zhu J, Han S. Lipidomic Profiling of Human Milk Derived Exosomes and Their
1135 Emerging Roles in the Prevention of Necrotizing Enterocolitis. Mol Nutr Food
1136 Res. 2021;65(10):e2000845. Epub 2021/03/15. doi: 10.1002/mnfr.202000845.
1137 PubMed PMID: 33715285.
1138 79. Yan X, Liu L, Yao S, Chen Y, Yu Q, Jiang C, Chen W, Chen X, Han S.
1139 LncRNA and mRNA profiles of human milk-derived exosomes and their possible
1140 roles in protecting against necrotizing enterocolitis. Food Funct.
1141 2022;13(24):12953-65. Epub 2022/12/01. doi: 10.1039/d2fo01866g. PubMed
1142 PMID: 36448375.
1143 80. Bickmore DC, Miklavcic JJ. Characterization of Extracellular Vesicles
1144 Isolated From Human Milk Using a Precipitation-Based Method. Front Nutr.

1145 2020;7:22. Epub 2020/04/02. doi: 10.3389/fnut.2020.00022. PubMed PMID:
1146 32232046; PMCID: PMC7082312.
1147 81. Kupsco A, Prada D, Valvi D, Hu L, Petersen MS, Coull B, Grandjean P,
1148 Weihe P, Baccarelli AA. Human milk extracellular vesicle miRNA expression and
1149 associations with maternal characteristics in a population-based cohort from the
1150 Faroe Islands. Sci Rep. 2021;11(1):5840. Epub 2021/03/14. doi:
1151 10.1038/s41598-021-84809-2. PubMed PMID: 33712635; PMCID: PMC7970999.
1152 82. Soares Martins T, Catita J, Martins Rosa I, O ABdCES, Henriques AG.
1153 Exosome isolation from distinct biofluids using precipitation and column-based
1154 approaches. PLoS One. 2018;13(6):e0198820. Epub 2018/06/12. doi:
1155 10.1371/journal.pone.0198820. PubMed PMID: 29889903; PMCID:
1156 PMC5995457 PLOS ONE policies, on sharing data and materials.
1157 83. Lobb RJ, Becker M, Wen SW, Wong CS, Wiegmans AP, Leimgruber A,
1158 Moller A. Optimized exosome isolation protocol for cell culture supernatant and
1159 human plasma. J Extracell Vesicles. 2015;4:27031. Epub 2015/07/22. doi:
1160 10.3402/jev.v4.27031. PubMed PMID: 26194179; PMCID: PMC4507751.
1161 84. Tan XH, Fang D, Xu YD, Nan TG, Song WP, Gu YY, Gu SJ, Yuan YM,
1162 Xin ZC, Zhou LQ, Guan RL, Li XS. Skimmed Bovine Milk-Derived Extracellular
1163 Vesicles Isolated via "Salting-Out": Characterizations and Potential Functions as
1164 Nanocarriers. Front Nutr. 2021;8:769223. Epub 2021/11/16. doi:
1165 10.3389/fnut.2021.769223. PubMed PMID: 34778348; PMCID: PMC8582325.
1166 85. Wijenayake S, Eisha S, Tawhidi Z, Pitino MA, Steele MA, Fleming AS,
1167 McGowan PO. Comparison of methods for pre-processing, exosome isolation,
1168 and RNA extraction in unpasteurized bovine and human milk. PLoS One.
1169 2021;16(9):e0257633. Epub 2021/10/01. doi: 10.1371/journal.pone.0257633.
1170 PubMed PMID: 34591894; PMCID: PMC8483318.
1171 86. Zlotogorski-Hurvitz A, Dayan D, Chaushu G, Korvala J, Salo T, Sormunen
1172 R, Vered M. Human saliva-derived exosomes: comparing methods of isolation. J
1173 Histochem Cytochem. 2015;63(3):181-9. Epub 2014/12/05. doi:
1174 10.1369/0022155414564219. PubMed PMID: 25473095; PMCID: PMC4340734.
1175 87. Taylor DD, Shah S. Methods of isolating extracellular vesicles impact
1176 down-stream analyses of their cargoes. Methods. 2015;87:3-10. Epub
1177 2015/03/15. doi: 10.1016/j.ymeth.2015.02.019. PubMed PMID: 25766927.
1178 88. Leiferman A, Shu J, Upadhyaya B, Cui J, Zempleni J. Storage of
1179 Extracellular Vesicles in Human Milk, and MicroRNA Profiles in Human Milk
1180 Exosomes and Infant Formulas. J Pediatr Gastroenterol Nutr. 2019;69(2):235-8.
1181 Epub 2019/06/07. doi: 10.1097/MPG.0000000000002363. PubMed PMID:
1182 31169664; PMCID: PMC6658346.
1183 89. Wesolowska A, Sinkiewicz-Darol E, Barbarska O, Bernatowicz-Lojko U,
1184 Borszewska-Kornacka MK, van Goudoever JB. Innovative Techniques of
1185 Processing Human Milk to Preserve Key Components. Nutrients. 2019;11(5).
1186 Epub 2019/05/30. doi: 10.3390/nu11051169. PubMed PMID: 31137691; PMCID:
1187 PMC6566440.
1188 90. Peila C, Moro GE, Bertino E, Cavallarin L, Giribaldi M, Giuliani F, Cresi F,
1189 Coscia A. The Effect of Holder Pasteurization on Nutrients and Biologically-
1190 Active Components in Donor Human Milk: A Review. Nutrients. 2016;8(8). Epub

1191 2016/08/05. doi: 10.3390/nu8080477. PubMed PMID: 27490567; PMCID:
1192 PMC4997390.
1193 91. Torrez Lamberti MF, Parker LA, Gonzalez CF, Lorca GL. Pasteurization of
1194 human milk affects the miRNA cargo of EVs decreasing its immunomodulatory
1195 activity. Sci Rep. 2023;13(1):10057. Epub 2023/06/22. doi: 10.1038/s41598-023-
1196 37310-x. PubMed PMID: 37344543; PMCID: PMC10284810.
1197 92. Kleinjan M, van Herwijnen MJ, Libregts SF, van Neerven RJ, Feitsma AL,
1198 Wauben MH. Regular Industrial Processing of Bovine Milk Impacts the Integrity
1199 and Molecular Composition of Extracellular Vesicles. J Nutr. 2021;151(6):1416-
1200 25. Epub 2021/03/27. doi: 10.1093/jn/nxab031. PubMed PMID: 33768229.
1201 93. Smyczynska U, Bartlomiejczyk MA, Stanczak MM, Sztromwasser P,
1202 Wesolowska A, Barbarska O, Pawlikowska E, Fendler W. Impact of processing
1203 method on donated human breast milk microRNA content. PLoS One.
1204 2020;15(7):e0236126. Epub 2020/07/16. doi: 10.1371/journal.pone.0236126.
1205 PubMed PMID: 32667939; PMCID: PMC7363072.
1206 94. Zonneveld MI, Brisson AR, van Herwijnen MJ, Tan S, van de Lest CH,
1207 Redegeld FA, Garssen J, Wauben MH, Nolte-'t Hoen EN. Recovery of
1208 extracellular vesicles from human breast milk is influenced by sample collection
1209 and vesicle isolation procedures. J Extracell Vesicles. 2014;3. Epub 2014/09/11.
1210 doi: 10.3402/jev.v3.24215. PubMed PMID: 25206958; PMCID: PMC4139932.
1211 95. Kim BJ, Lueangsakulthai J, Sah BNP, Scottoline B, Dallas DC.
1212 Quantitative Analysis of Antibody Survival across the Infant Digestive Tract Using
1213 Mass Spectrometry with Parallel Reaction Monitoring. Foods. 2020;9(6). Epub
1214 2020/06/13. doi: 10.3390/foods9060759. PubMed PMID: 32526824; PMCID:
1215 PMC7353590.
1216 96. Fafian-Labora JA, Rodriguez-Navarro JA, O'Loghlen A. Small Extracellular
1217 Vesicles Have GST Activity and Ameliorate Senescence-Related Tissue
1218 Damage. Cell Metab. 2020;32(1):71-86 e5. Epub 2020/06/24. doi:
1219 10.1016/j.cmet.2020.06.004. PubMed PMID: 32574561; PMCID: PMC7342013.
1220 97. Takov K, Yellon DM, Davidson SM. Confounding factors in vesicle uptake
1221 studies using fluorescent lipophilic membrane dyes. J Extracell Vesicles.
1222 2017;6(1):1388731. Epub 2017/12/01. doi: 10.1080/20013078.2017.1388731.
1223 PubMed PMID: 29184625; PMCID: PMC5699187.
1224 98. Ros-Baro A, Lopez-Iglesias C, Peiro S, Bellido D, Palacin M, Zorzano A,
1225 Camps M. Lipid rafts are required for GLUT4 internalization in adipose cells. Proc
1226 Natl Acad Sci U S A. 2001;98(21):12050-5. Epub 2001/10/11. doi:
1227 10.1073/pnas.211341698. PubMed PMID: 11593015; PMCID: PMC59765.
1228 99. Mettlen M, Platek A, Van Der Smissen P, Carpentier S, Amyere M,
1229 Lanzetti L, de Diesbach P, Tyteca D, Courtoy PJ. Src triggers circular ruffling and
1230 macropinocytosis at the apical surface of polarized MDCK cells. Traffic.
1231 2006;7(5):589-603. Epub 2006/04/29. doi: 10.1111/j.1600-0854.2006.00412.x.
1232 PubMed PMID: 16643281.
1233

Human milk extracellular vesicles survive neonatal digestion to be absorbed by neonatal intestinal epithelial cells

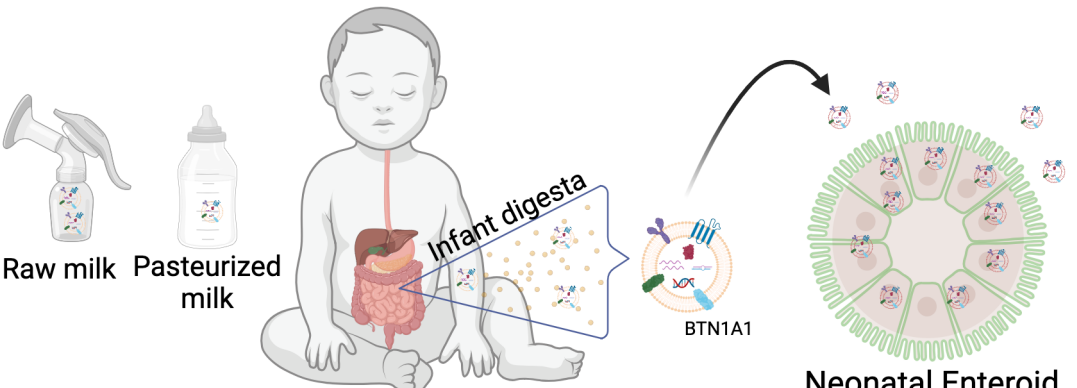

Graphical Abstract

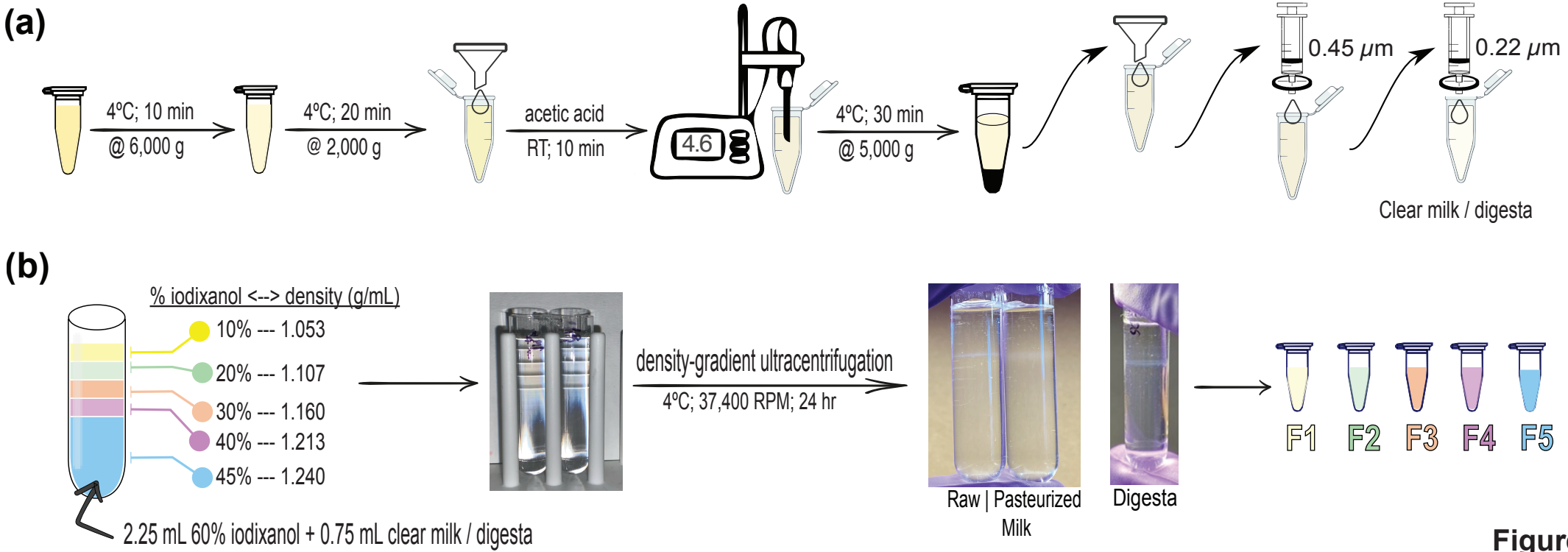
(a)
4ºC; 10 min
@ 6,000 g
4ºC; 20 min
@ 2,000 g
acetic acid
RT; 10 min
4.6
4ºC; 30 min
@ 5,000 g
0.45 μm
0.22 μm
Clear milk / digesta
(b)
% iodixanol <--> density (g/mL)
10% --- 1.053
20% --- 1.107
30% --- 1.160
40% --- 1.213
45% --- 1.240
2.25 mL 60% iodixanol + 0.75 mL clear milk / digesta
density-gradient ultracentrifugation
4ºC; 37,400 RPM; 24 hr
Raw | Pasteurized Milk
Digesta
F1
F2
F3
F4
F5

Figure 1

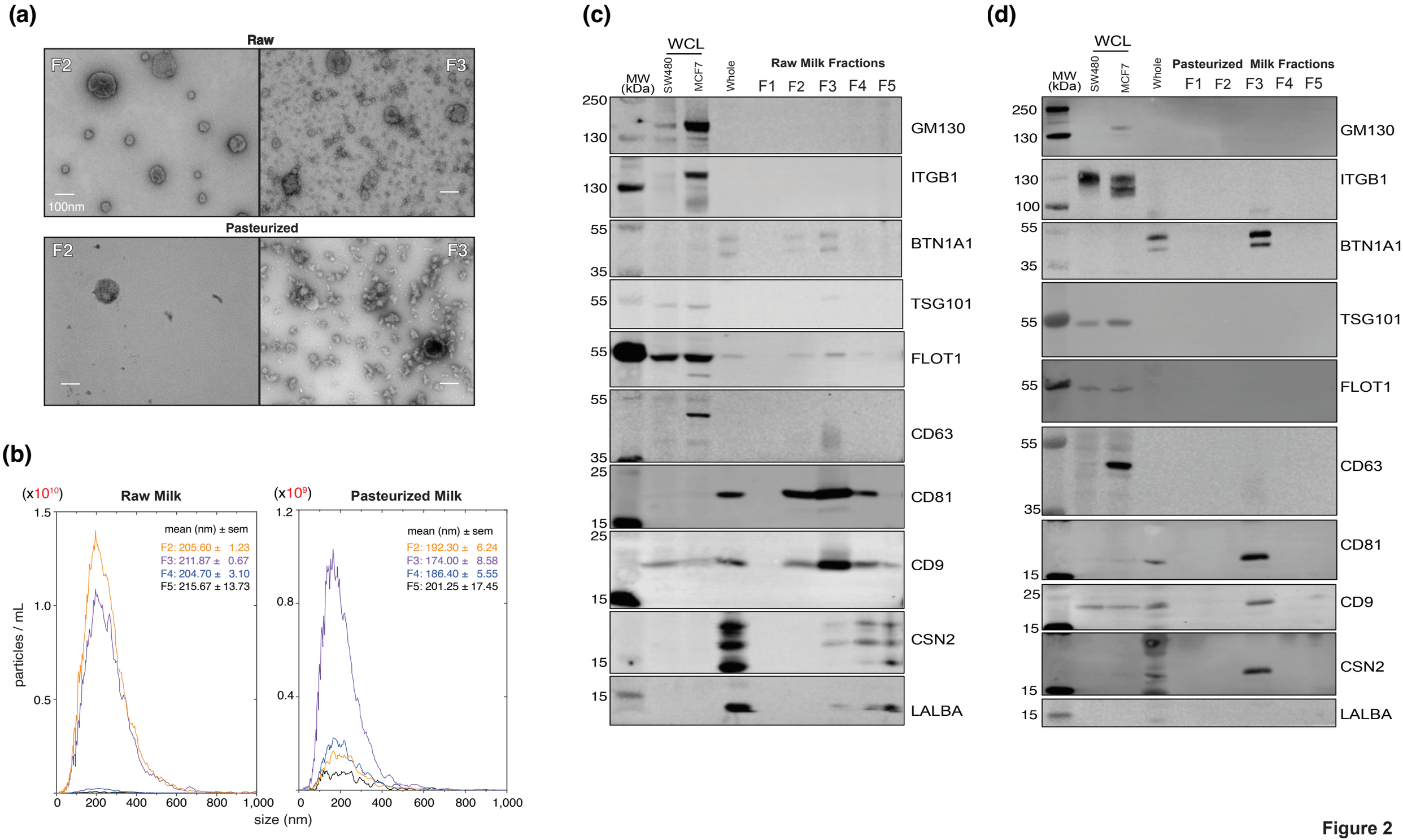
(a)
Raw
F2
F3
100nm
Pasteurized
F2
F3
(b)
(x10¹⁰)
Raw Milk
mean (nm) ± sem
F2: 205.60 ± 1.23
F3: 211.87 ± 0.67
F4: 204.70 ± 3.10
F5: 215.67 ± 13.73
(x10⁹)
Pasteurized Milk
mean (nm) ± sem
F2: 192.30 ± 6.24
F3: 174.00 ± 8.58
F4: 186.40 ± 5.55
F5: 201.25 ± 17.45
particles / mL
size (nm)
(c)
WCL
MW (kDa)
SW480
MCF7
Whole
Raw Milk Fractions
F1 F2 F3 F4 F5
GM130
ITGB1
BTN1A1
TSG101
FLOT1
CD63
CD81
CD9
CSN2
LALBA
(d)
WCL
MW (kDa)
SW480
MCF7
Whole
Pasteurized Milk Fractions
F1 F2 F3 F4 F5
GM130
ITGB1
BTN1A1
TSG101
FLOT1
CD63
CD81
CD9
CSN2
LALBA

Figure 2

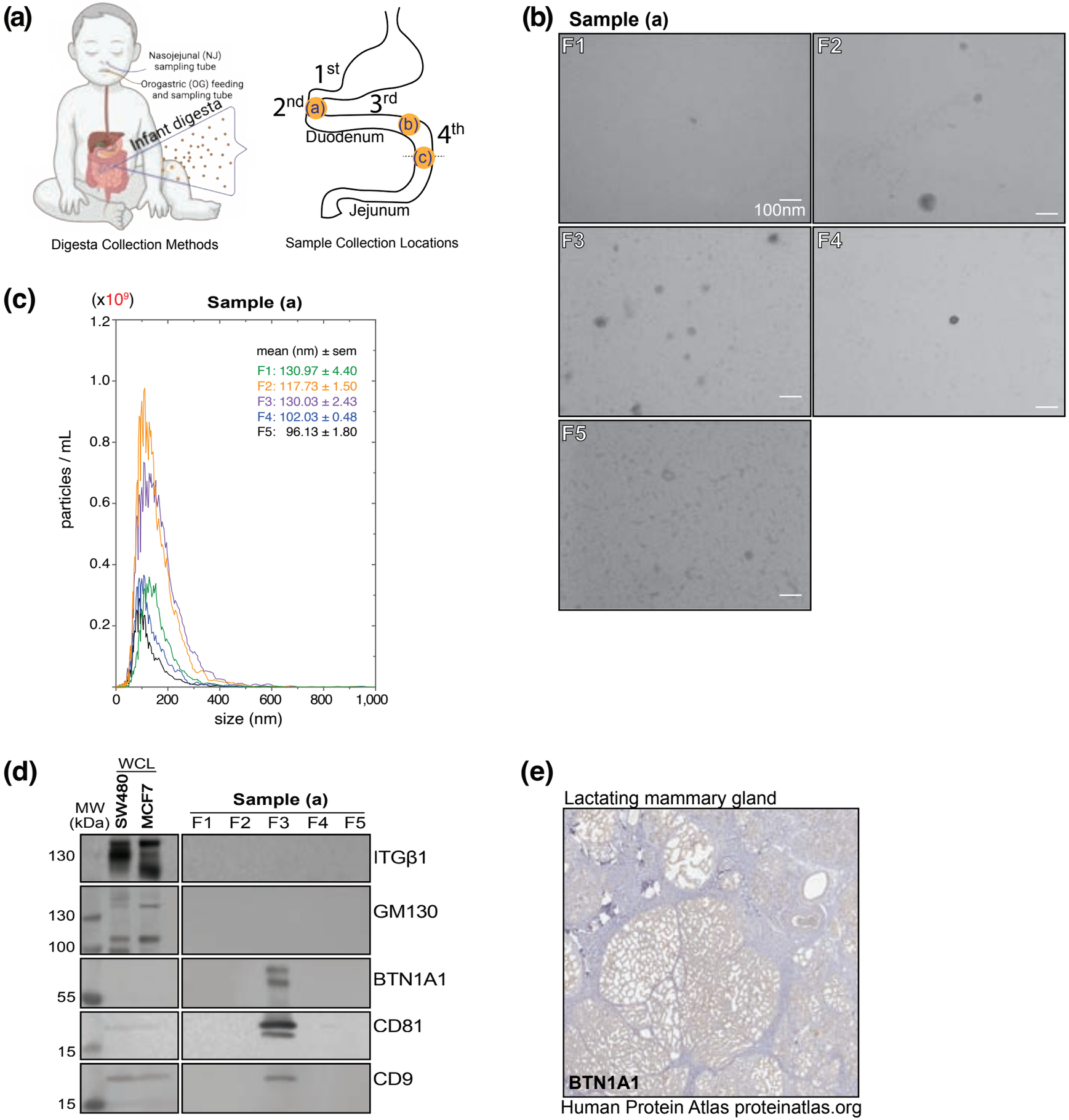
(a)
Nasojejunal (NJ) sampling tube
Orogastric (OG) feeding and sampling tube
Infant digesta
Digesta Collection Methods
1st
2nd
3rd
4th
(a)
(b)
(c)
Duodenum
Jejunum
Sample Collection Locations
(b)
Sample (a)
F1
F2
F3
F4
F5
100nm
(c)
(x10⁹)
Sample (a)
mean (nm) ± sem
F1: 130.97 ± 4.40
F2: 117.73 ± 1.50
F3: 130.03 ± 2.43
F4: 102.03 ± 0.48
F5: 96.13 ± 1.80
particles / mL
size (nm)
(d)
WCL
MW (kDa)
SW480
MCF7
Sample (a)
F1 F2 F3 F4 F5
130
ITGβ1
130
100
GM130
55
BTN1A1
15
CD81
15
CD9
(e)
Lactating mammary gland
BTN1A1
Human Protein Atlas proteinatlas.org

Figure 3

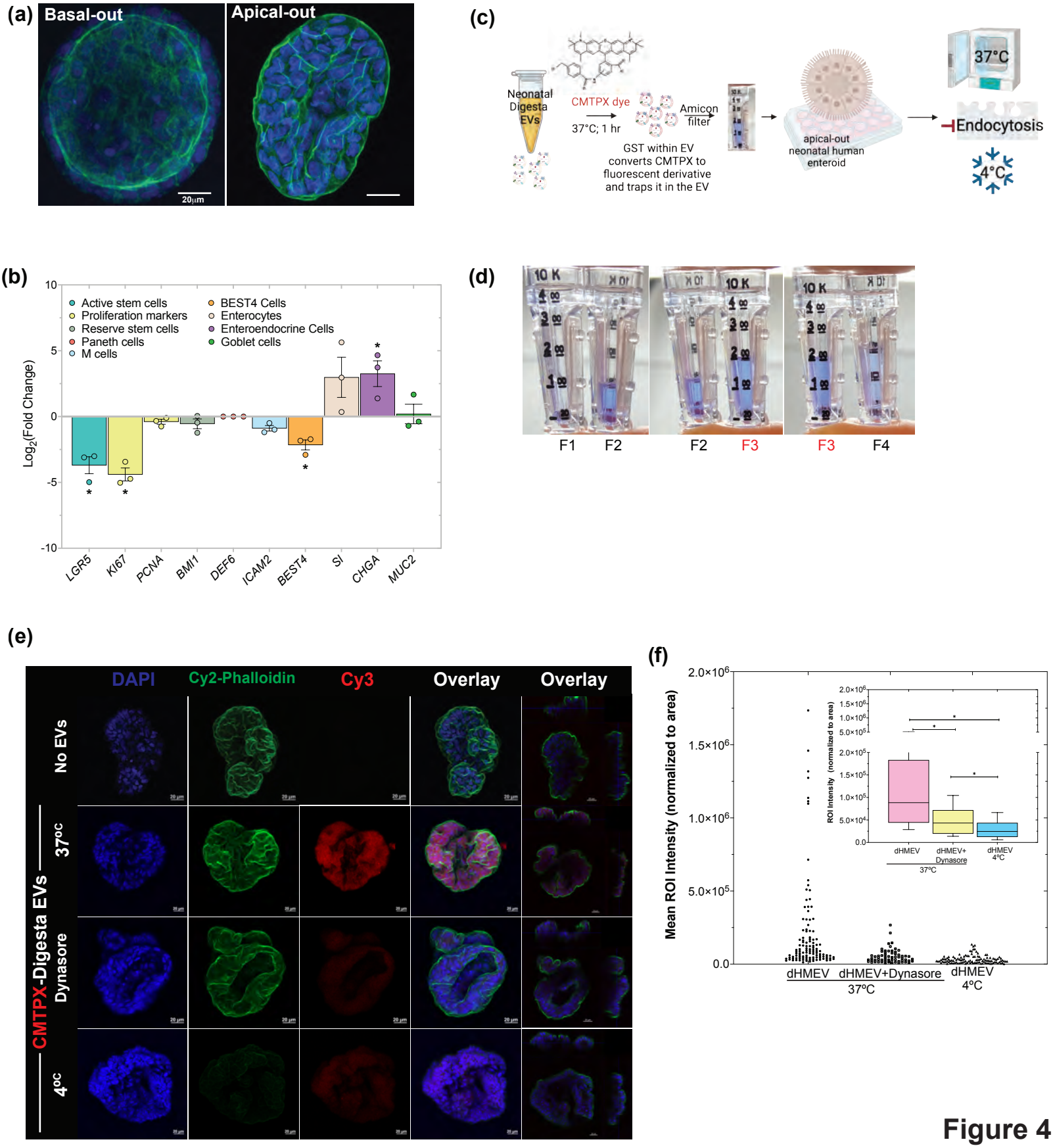
(a)
Basal-out
Apical-out
20µm
(c)
Neonatal Digesta EVs
CMTPX dye
37°C; 1 hr
Amicon filter
GST within EV converts CMTPX to fluorescent derivative and traps it in the EV
apical-out neonatal human enteroid
37°C
Endocytosis
4°C
(b)
Active stem cells
Proliferation markers
Reserve stem cells
Paneth cells
M cells
BEST4 Cells
Enterocytes
Enteroendocrine Cells
Goblet cells
Log2(Fold Change)
10
5
0
-5
-10
LGR5
KI67
PCNA
BMI1
DEF6
ICAM2
BEST4
SI
CHGA
MUC2
(d)
10 K
F1
F2
F2
F3
F3
F4
(e)
DAPI
Cy2-Phalloidin
Cy3
Overlay
Overlay
No EVs
CMTPX-Digesta EVs
37°C
Dynasore
4°C
(f)
Mean ROI Intensity (normalized to area)
2.0×10^6
1.5×10^6
1.0×10^6
5.0×10^5
0.0
dHMEV
dHMEV+Dynasore
dHMEV
37°C
4°C
ROI Intensity (normalized to area)
dHMEV+ Dynasore

Figure 4

Table 1. Human milk and digesta sample demographics.

Raw Human Milk	**#1**	**#2**	**#3**
Age	36	25	37
Pregnancy	3rd	3rd	6th
Delivery	3rd	3rd	1st
Mode of delivery	cesarean	vaginal	cesarean
Weeks post-delivery	20	4	18
Collection Method	Hospital-grade electric pump		
Storage	Frozen	Frozen	Frozen
Newborn			
Sex	female	male	female
Birth weight (g)	885	710	723
Gestational age (wks)	27 3/7	24 3/7	23 5/7
Pasteurized Human Donor Milk Source	**Prolact HM®**	**NW Mothers Milk Bank Batch A**	**NW Mothers Milk Bank Batch B**
Pasteurization	Vat	Holder	Holder
Storage	Frozen	Frozen	Frozen
Digesta (d)	**d(a)**	**d(b)**	**d(c)**
Feed	Raw HM	Raw HM	Raw HM
Sex	Male	Male	Male
Gestational age (wks)	44 4/7	39 1/7	44 1/7
Collection Location	2nd duo	3rd/4th duo	4th duo/prox jej
Sample Storage	Frozen	Frozen	Frozen